AD-A135 304 ENVIRONMENTAL DURABILITY OF ALUMINUM ADHESIVE JOINTS PROTECTED WITH HYDRATION INHIBITORS(U) MARTIN MARIETTA LABS BALTIMORE MD G D DAVIS ET AL. NOV 83 1/2

UNCLASSIFIED MML-TR-83-34C N00014-80-C-0718 F/G 11/1 NL

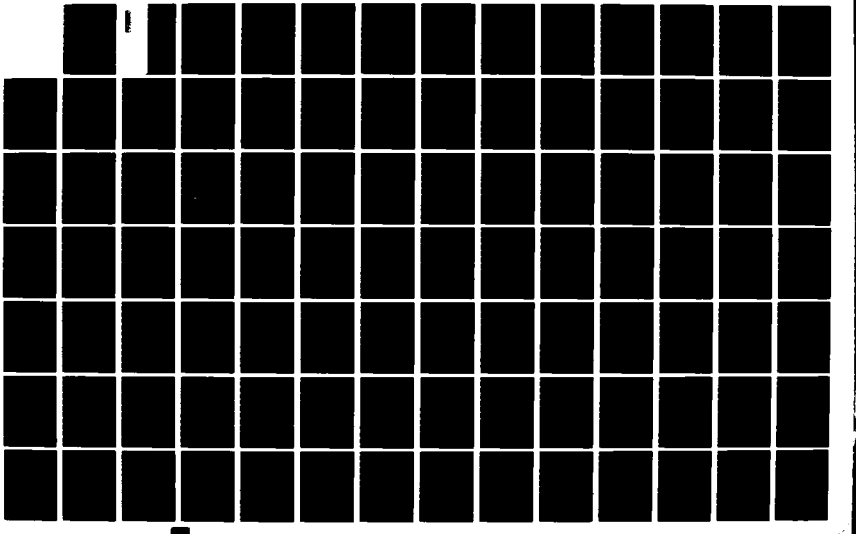

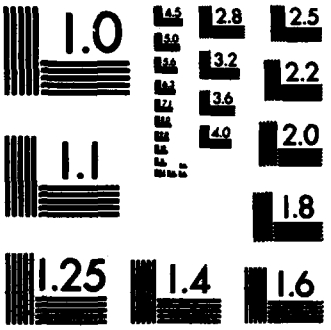

(12)

MARTIN MARIETTA

Martin Marietta
Laboratories

MML TR 83-34c

ENVIRONMENTAL DURABILITY OF ALUMINUM ADHESIVE JOINTS PROTECTED WITH HYDRATION INHIBITORS

End-of-Third-Year Report
July 1, 1982 to June 30, 1983

November 1983

Prepared for:

Department of the Navy
Office of Naval Research
Arlington, Virginia 22217

Prepared by:

Martin Marietta Laboratories
1450 South Rolling Road
Baltimore, Maryland 21227

Under
ONR Contract N00014-80-C-0718

SECURITY CLASSIFICATION OF THIS PAGE *(When Data Entered)*

REPORT DOCUMENTATION PAGE

READ INSTRUCTIONS BEFORE COMPLETING FORM

1. REPORT NUMBER	2. GOVT ACCESSION NO. AD-A135 304
3. RECIPIENT'S CATALOG NUMBER	
4. TITLE *(and Subtitle)* Environmental Durability of Aluminum Adhesive Joints Protected with Hydration Inhibitors	5. TYPE OF REPORT & PERIOD COVERED End-of-Third-Year Report
	6. PERFORMING ORG. REPORT NUMBER MML TR 83-34c
7. AUTHOR(s) G. D. Davis, J. S. Ahearn, J. D. Venables	8. CONTRACT OR GRANT NUMBER(s) N00014-80-C-0718
9. PERFORMING ORGANIZATION NAME AND ADDRESS Martin Marietta Laboratories, 1450 South Rolling Road, Baltimore, Maryland 21227	10. PROGRAM ELEMENT, PROJECT, TASK AREA & WORK UNIT NUMBERS
11. CONTROLLING OFFICE NAME AND ADDRESS Department of the Navy, Office of Naval Research, Arlington, Virginia 22217	12. REPORT DATE November 1983
	13. NUMBER OF PAGES 29
14. MONITORING AGENCY NAME & ADDRESS *(if different from Controlling Office)* Baltimore DCAS Management Area, 300 East Joppa Road, Room 200, Towson, Maryland 21204	15. SECURITY CLASS. *(of this report)*
	15a. DECLASSIFICATION/DOWNGRADING SCHEDULE

16. DISTRIBUTION STATEMENT *(of this Report)*

Unlimited distribution.

Accession For
NTIS GRA&I ☑
DTIC TAB ☐
Unannounced ☐
Justification
By
Distribution/
Availability Codes
Dist | Avail and/or Special
A-1

17. DISTRIBUTION STATEMENT *(of the abstract entered in Block 20, if different from Report)*

18. SUPPLEMENTARY NOTES

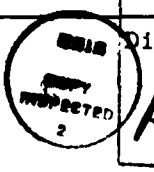

19. KEY WORDS *(Continue on reverse side if necessary and identify by block number)*

Adhesive bonding, organic inhibitors, mechanical testing, aluminum, surface behavior diagrams.

20. ABSTRACT *(Continue on reverse side if necessary and identify by block number)*

The adsorption of selected, organic, hydration inhibitors onto and the subsequent hydration of Forest Products Laboratory (FPL)-etched surfaces has been studied using X-ray photoelectron spectroscopy (XPS) and surface behavior diagrams (SBD's) supplemented by inelastic electron tunnelling spectroscopy (IETS) and Fourier Transform Infrared Spectroscopy (FTIR). The results indicate that nitrilotris methylene phosphonic acid (NTMP) and related compounds

DD FORM 1 JAN 73 1473

SECURITY CLASSIFICATION OF THIS PAGE *(When Data Entered)*

adsorb to the alumina surface via the POH bonds of the phosphonic acid groups, resulting in a displacement of water normally adsorbed onto the surface. A model of adsorption was developed that suggests that at very low treatment solution concentrations (~ 1 ppm) only one leg of the NTMP molecule adsorbs onto the surface although at higher concentrations (~ 100 ppm) all three legs do. Hydration is a three-step process: 1) a reversible physisorption of water, 2) a slow dissolution of the inhibitor followed by a rapid hydration of the freshly exposed Al_2O_3 to boehmite AlOOH, and 3) a further hydration of the AlOOH to bayerite $Al(OH)_3$. It is during the second step that bond failure occurs with the dissolution of the inhibitor being the rate limiting reaction. Analysis of the adsorption, hydration, and wedge tests results using different inhibitors suggests four criteria of an inhibitor to promote good bond performance: 1) occupation of all active sites on the Al_2O_3 surface, 2) strong inhibitor surface bonds, 3) insolubility of the resulting inhibitor-aluminum complex in aqueous solutions, and 4) compatibility with the adhesive/primer.

MML TR 83-34c

ENVIRONMENTAL DURABILITY OF ALUMINUM ADHESIVE JOINTS PROTECTED WITH HYDRATION INHIBITORS

End-of-Third-Year Report on
ONR Contract N00014-80-C-0718

November 1983

Prepared for:

Department of the Navy
Office of Naval Research
Arlington, Virginia 22217

Prepared by:

G. D. Davis, J. S. Ahearn, and J. D. Venables
Martin Marietta Laboratories
1450 South Rolling Road
Baltimore, Maryland 21227

G. D. Davis
Principal Investigator

TABLE OF CONTENTS

LIST OF FIGURES

FIGURES (continued)

LIST OF TABLES

I. INTRODUCTION

The performance of adhesively bonded aluminum structures is judged primarily by the initial bond strength and by the long-term durability of the bond. The high initial bond strength provided by commercial aerospace bonding processes[1,2] is a consequence of the microscopically rough aluminum oxide formed during the etching or anodization treatment. When polymeric adhesive is added, it penetrates the oxide pores and surrounds the oxide whiskers, resulting in a physical interlocking that ensures a much stronger bond than that possible with a smooth oxide surface.[3,4]

The oxide morphology also partially governs long-term bond durability in moist environments in that the mechanical interlocking of an adhesive and a rough aluminum oxide stays high even if their chemical interaction is disrupted. In these cases, a crack can propagate only if this interlocking is destroyed or if the failure occurs cohesively or along another interface. Work at Martin Marietta Laboratories has shown that crack propagation occurs as the aluminum oxide hydrates to the oxyhydroxide boehmite, allowing failure either at the boehmite/metal interface or at the boehmite/adhesive interface.[5-7]

These findings have prompted us to investigate methods to inhibit the oxide-to-hydroxide conversion process and thereby to improve the long-term durability of adhesively bonded aluminum structures. One such procedure is to treat a Forest Products Laboratory (FPL) sodium dichromate/sulfuric-acid-etched adherend with certain organic acids (amino phosphonates). These surfaces, with a saturation inhibitor coverage of

approximately one monolayer, exhibit a much higher resistance to hydration (up to two orders of magnitude) than untreated FPL surfaces and have a corresponding increase in the long-term bond durability.[8]

In the previous years of this program (ONR N00014-80-C-0718),[6,9] we examined the mechanical properties of adhesive bonds formed with FPL and phosphoric-acid-anodized (PAA) adherends treated with hydration inhibitors, particularly nitrilotris methylene phosphonic acid (NTMP, $N[CH_2PO(OH)_2]_3$). We showed that: 1) NTMP-treated FPL bonds and PAA bonds exhibited similar long-term durability; 2) the durability of NTMP-treated PAA bonds was better then untreated PAA bonds; and 3) an inhibitor's effectiveness depended both on its ability to inhibit the oxide-to-hydroxide conversion and on its compatibility with the adhesive.

In the continuation of this program, we have used X-ray photoelectron spectroscopy (XPS), Fourier-Transform Infrared Spectroscopy (FTIR), and/or Inelastic Tunnelling Spectroscopy (IETS) to examine the adsorption process of NTMP and similar inhibitors onto FPL-prepared adherends as well as the hydration behavior of the inhibited surfaces. Using the models for hydration thus developed, we have attempted to modify the inhibitor molecule to enhance its effectiveness in stabilizing the aluminum oxide and improving bond durability.

These adsorption and hydration processes were studied with the use of surface behavior diagrams (SBD's),[10,11] a new method of analysis of quantitative surface-sensitive results recently developed at the Laboratories. These diagrams display graphically the changes in the surface composition as a function of reaction time, solution concentration,

anodization voltage, depth in the sample, or other parameters of interest. The SBD's resemble ternary or quaternary phase diagrams in that they represent the surface composition as the sum of the compositions of three or four basis compounds. They differ, however, in that they display compositional data rather than structural data. In addition, the equilibrium condition is relaxed for SBD's, so that the surface can be described during non-equilibrium states such as hydration.

II. EXPERIMENT

A. SURFACE PREPARATION

Bare test coupons and panels of 2024 Al were degreased by 15 minute immersion in an agitated solution of Turco 4215* (44 g/l) at 65°C and then rinsed in distilled, deionized water. Degreasing was followed by a standard FPL treatment, consisting of a 15-minute immersion in an agitated aqueous solution of sodium dichromate dihydrate (60 g/l) and sulfuric acid (17% v/v) held at 65°C, after which samples were rinsed in distilled, deionized water and air dried. Some FPL-treated panels were then treated using the PAA process. These panels were anodized in a 10 wt% phosphoric acid solution at a potential of 10 V for 20 minutes, rinsed in distilled, de-ionized water, and air dried.

The coupons were immersed for 30 minutes in a dilute aqueous solution of the inhibitor held at room temperature. Solution concentrations ranged from 0.1 to 500 ppm for the adsorption experiments and from 100 to 300 ppm for the hydration studies and the wedge tests. In a separate experiment, the time of immersion in a 300 ppm NTMP solution was varied from 5 seconds to 30 minutes. The samples were then thoroughly rinsed in distilled de-ionized water, forced-air dried, and stored in a dessicator until analysis.

Samples used in the hydration experiments were suspended vertically in a Blue M humidity chamber and were exposed to air saturated with water

---

* An alkaline cleaning agent manufactured by Turco Products.

vapor at 50°C. The samples were then removed at different intervals, dried with forced air, and also stored in a dessicator.

Other coupons (6 x 6 x 0.125 in.) were bonded together using American Cyanamid FM 123-2 adhesive cured at 120°C and 40 psi for 1 hour. The bonded panels were cut into 1 x 6 in. test strips and a wedge (0.125-in. thick) was inserted between the two adherends to provide a stress at the bondline. After 1-hour equilibration at ambient conditions, the wedge-test samples were placed in a humidity chamber held at 60°C and 98% relative humidity. In order to determine the extent of crack propagation, we periodically removed the test pieces from the humidity chamber and examined them under an optical microscope, locating and marking the position of the crack front. When the test was complete, usually after 150 to 160 hours, calipers were used to measure the positions of these marks, which denote crack length as a function of time.

B. INHIBITOR PREPARATION

Most of the inhibitors investigated -- NTMP, amino methylene phosphonic acid [AMP, $H_2NCH_2PO(OH)_2$], and methylene phosphonic acid [MP, $CH_3PO(OH)_2$] -- are commercially available. One, (n-butyl) nitrilobis methylene phosphonic acid [(n Bu)NBMP, $n\text{-}C_4H_9N$ $[CH_2PO(OH)_2]$, was synthesized by allowing the hydrochloride salt of n-butylamine $[C_4H_9NH_2]$ to react with an aqueous solution of phosphorus acid $[H_3PO_3]$ and formaldehyde $[CH_2O]$. The solution was heated to 80°C with stirring before being evaporated to a viscous film which was filtered and washed with anhydrous ethanol and washed with ether. The crystals were air dried and further

dried in vacuo.[12] These crystals exhibited a melting point of 185-191°C and analytical elemental analysis results were in excellent agreement with calculated values (Table 1).

Table 1

Measured and Calculated Analysis for (n Bu) NBMP

	C	H	N	P
Measured	27.74	6.45	5.26	22.77
Calculated	27.59	6.51	5.36	23.75

C. SURFACE ANALYSIS

The surface chemistry was determined by XPS. Measurements were made on a Physical Electronics Model 548 spectrometer, which consists of a double-pass cylindrical mirror analyzer (CMA) with pre-retarding grids and a coaxial electron gun, a Mg anode X-ray source, a rasterable 5-keV sputter ion gun, a sample introduction device, and a gas-handling system used to backfill the chamber to 5×10^{-5} Torr Ar. Operating pressure was in the low 10^{-9} Torr range.

Atomic concentrations were determined from high-resolution (50-eV pass energy) spectra of the O1s, Al2p, and P2p peaks and sensitivity factors measured from standards on this instrument.[10]

The XPS measurements were sometimes supplemented by Auger electron spectroscopy (AES) and ion sputtering to obtain an elemental distribution with depth.

The atomic concentrations of O, Al, and P were converted to molar concentrations of Al_2O_3, inhibitor, and H_2O for the inhibitor-treated FPL

samples, using the following assumptions. All the P was assigned to the inhibitor, the Al was assigned to Al_2O_3, and enough O was used to satisfy the inhibitor and Al_2O_3 requirements. Any excess was assumed to be bonded to H as H_2O. For example, AlOOH has a composition equivalent to $Al_2O_3 + H_2O$ even though it is not a two-phase mixture of these compounds. The molar concentrations were then plotted on the appropriate SBD.

Additional measurements were obtained from IETS and FTIR tests. The IETS measurements performed at the University of Missouri by Dr. Henry White are discussed in the appended subcontractor's report. The FTIR measurements were obtained on a Nicolet 7199 spectrometer using the diffuse reflectance (DRIFT) technique. The reference material was KBr powder and the samples were mixtures of the material of interest and KBr.

III. RESULTS

A. ADSORPTION

The adsorption of NTMP upon FPL surfaces was studied as a function of solution concentration and, to a lesser extent, time of immersion. The dependence of the surface composition on solution concentration is shown in the Al_2O_3-NTMP-H_2O surface behavior diagram of Fig. 1. The solution concentration increases from left to right. The approximately horizontal position of the curve corresponds to the saturation coverage (P/Al ≈ 0.15) of approximately one monolayer reported earlier.[8,9] This adsorption process can be described as a displacement reaction during which the NTMP displaced water or hydroxyl groups initially bound to the aluminum oxide surface. In an adsorption process in which the water was not removed, the surface composition evolutionary path would be vertical, i.e., in the direction of the inhibitor.

Saturation coverage is rapidly achieved upon immersion. Figure 2 indicates that the NTMP layer has grown to the monolayer thickness in less than five seconds of treatment and remains at this level for up to thirty minutes of immersion.

Similar adsorption studies on the effect of solution concentration were made for AMP and (n Bu) NBMP on FPL and NTMP on PAA. The adsorption of the two inhibitors onto FPL (Figs. 3 and 4) are qualitatively similar to that of NTMP on FPL, i.e., a displacement reaction of the inhibitor in exchange for adsorbed water. Subtle apparent differences between the NTMP and AMP adsorption behavior, which are more evident in Fig. 5, will be

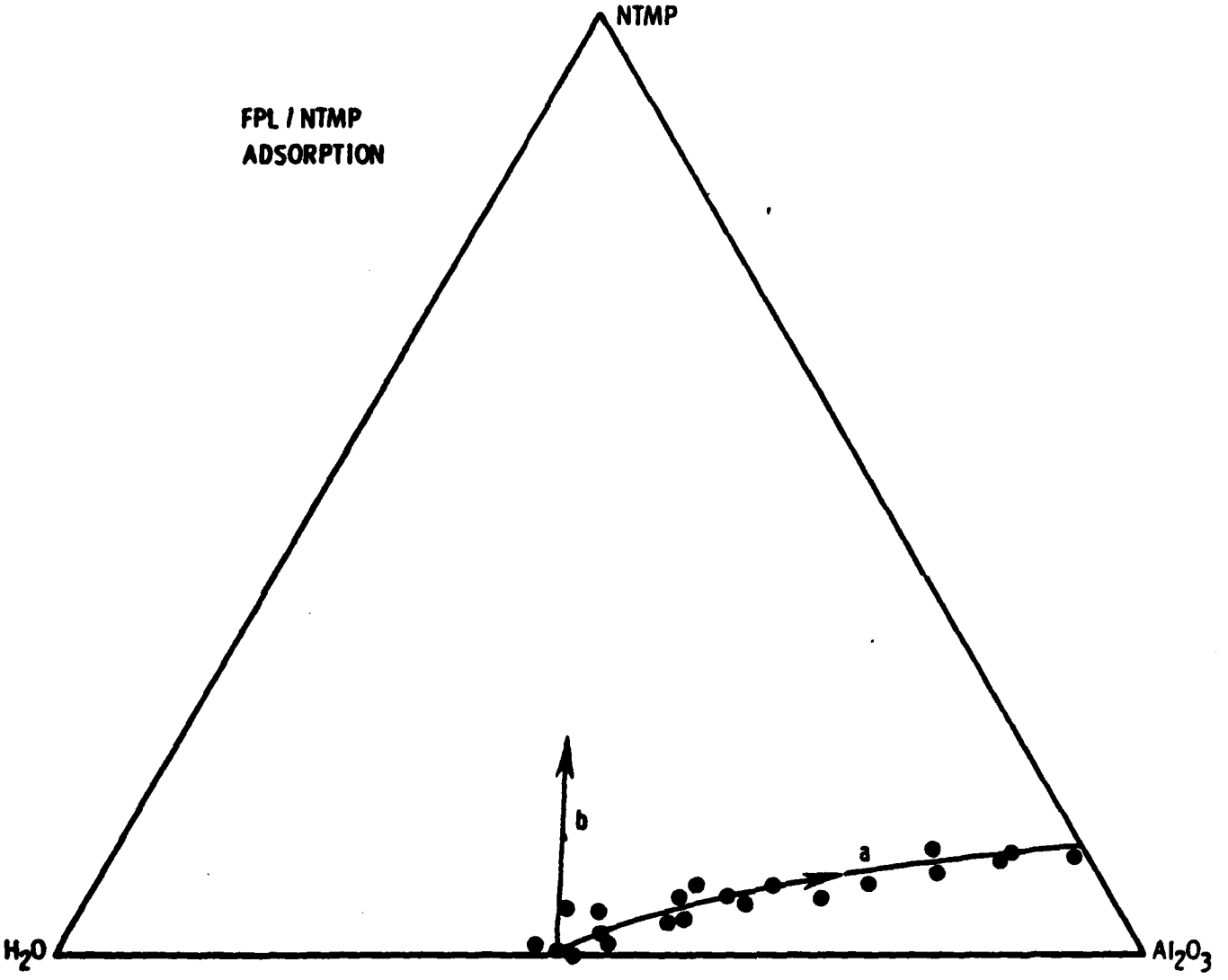

Figure 1. Al_2O_3-NTMP-H_2O SBD showing a) the surface composition of FPL-etched surfaces after immersion for 30 minutes in aqueous solutions of NTMP at concentrations ranging from 0.1 to 500 ppm, solution concentration increases from left to right, and b) the path representing no displacement of water.

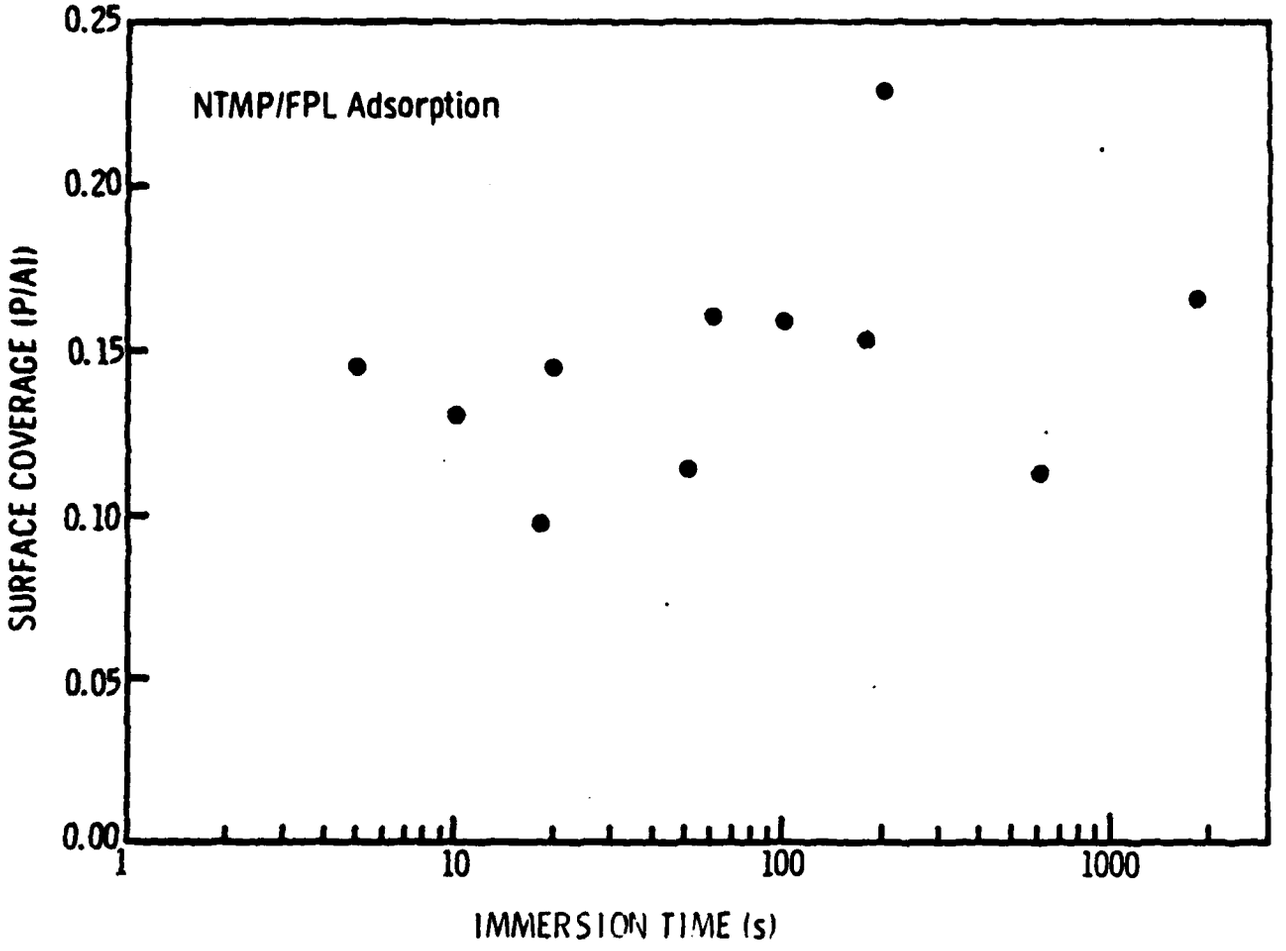

Figure 2. NTMP coverage (P/Al) of FPL-etched surfaces as a function of immersion time in a 300-ppm NTMP solution.

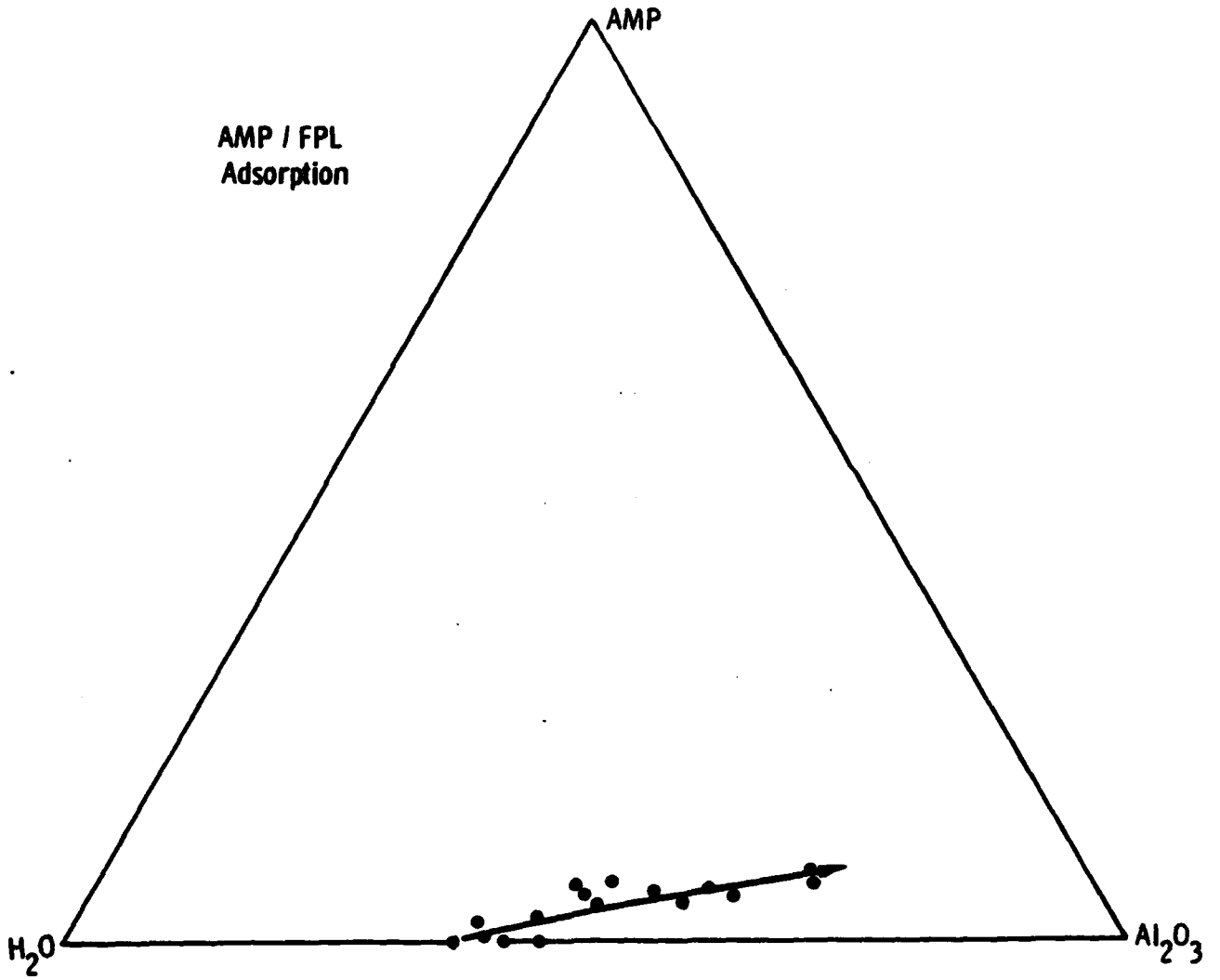

Figure 3. Al_2O_3-AMP-H_2O SBD showing the surface composition of FPL-etched surfaces after immersion in solutions of AMP at concentrations of 1 to 300 ppm.

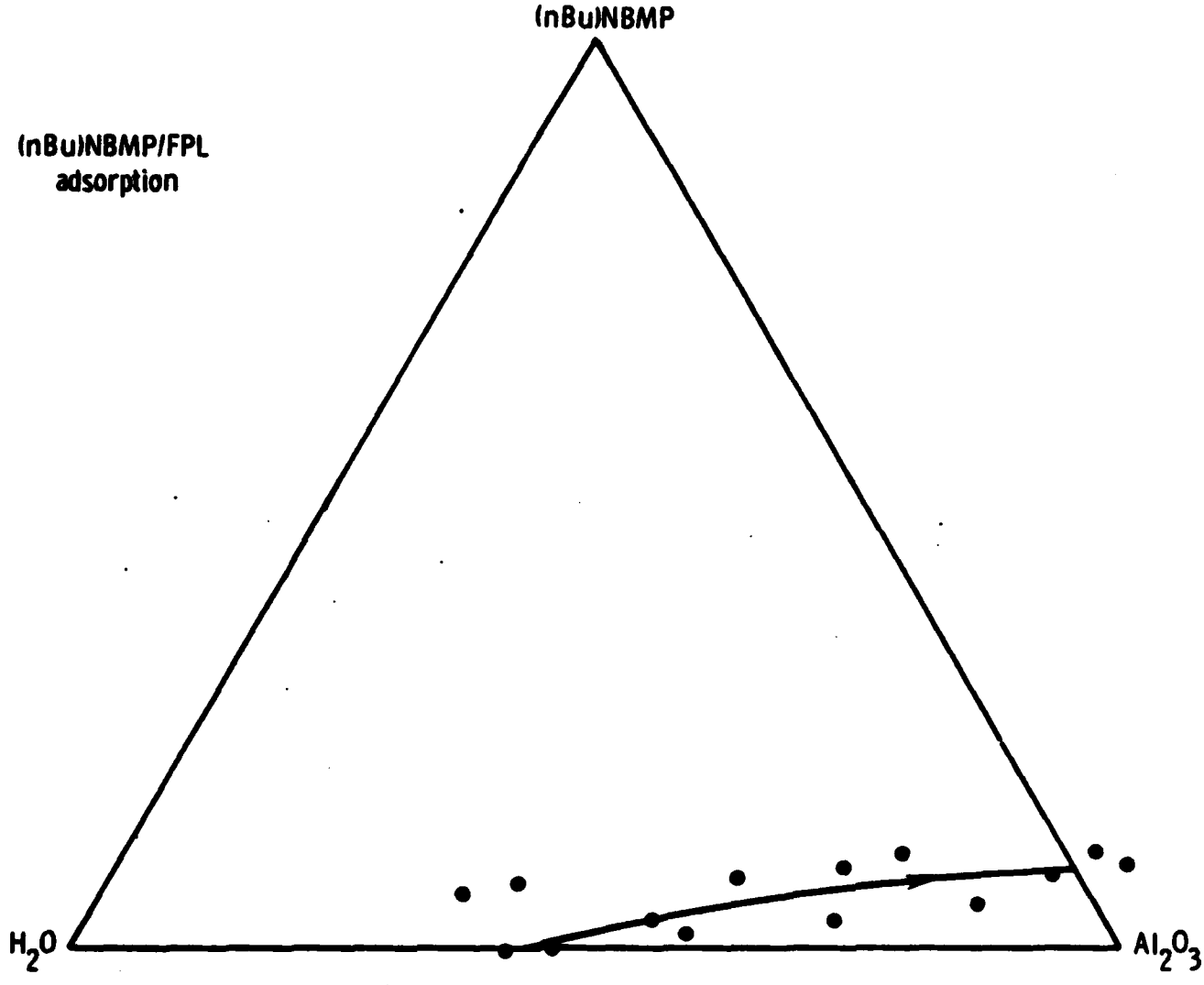

Figure 4. Al_2O_3-(n Bu) NBMP-H_2O SBD showing the surface composition of FPL-etched surfaces after immersion in solution of (n Bu) NBMP at concentrations of 1 to 300 ppm.

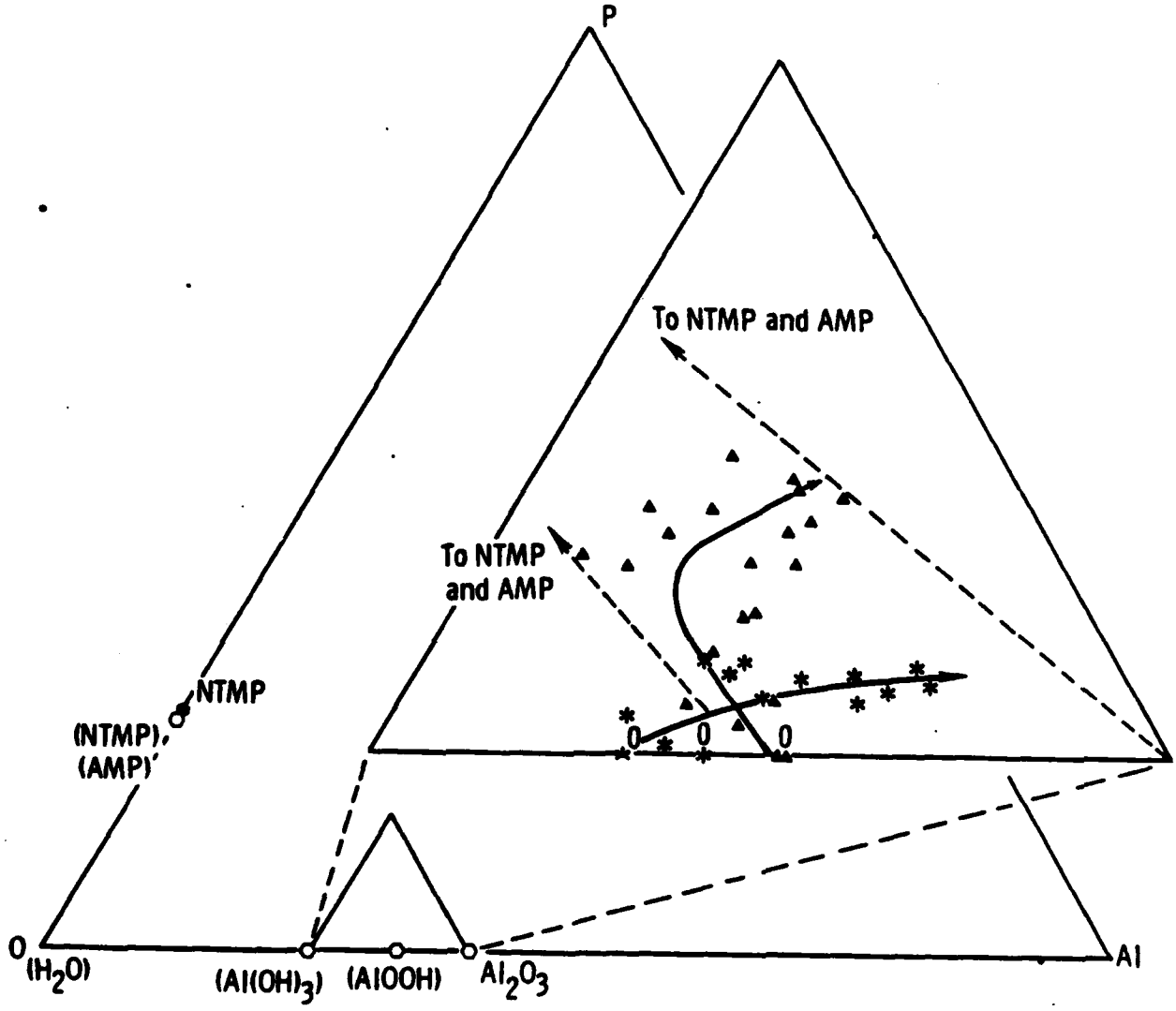

Figure 5. Al-P-O SBD showing the surface composition of FPL-etched surfaces after immersion in solutions of NTMP (triangles) or AMP (stars) at various concentrations. Open hexagons are calculated compositions. Compositions denoted by "0" represent surfaces not immersed in NTMP solutions.

discussed later (Section IV). The adsorption of NTMP onto PAA surfaces, in contrast, is considerably different from that of NTMP onto FPL surfaces as shown in Fig. 6. Here, because of the two different phosphorous states present (phosphate and phosphonic acid groups), the Al-P-O elemental SBD is shown. (The Al_2O_3-$AlPO_4$-H_2O and the Al_2O_3-NTMP-H_2O SBD's for PAA[10] and inhibited FPL surfaces, respectively, are subsets of this larger SBD.) Also, included in this SBD, for comparison purposes, is the evolution of the composition of FPL surfaces upon NTMP adsorption. Unlike the previous cases, the adsorption of NTMP onto PAA surfaces involves no displacement of water, but simply an addition of the inhibitor to the already dehydrated surface.

The FTIR spectrum of solid NTMP is shown in Fig. 7 and the assignments of the various peak absorbances are given in Table 2. Because of

Table 2

FTIR Band Assignments

	Wavenumbers (cm^{-1})	
Assignment	NTMP	Al-NTMP
OH	3500-2800	3500-2800
NH^+	3020	3026
OH	1653	1646
CH_2	1435	1434
P=O	1188-970	1160
Al-O		956
PO_3^{2-}	808-723	
P-O-Al		751

the high degree of symmetry in the molecule, the infrared spectrum is very weak and is comprised of broad bands. Analysis of the FTIR results

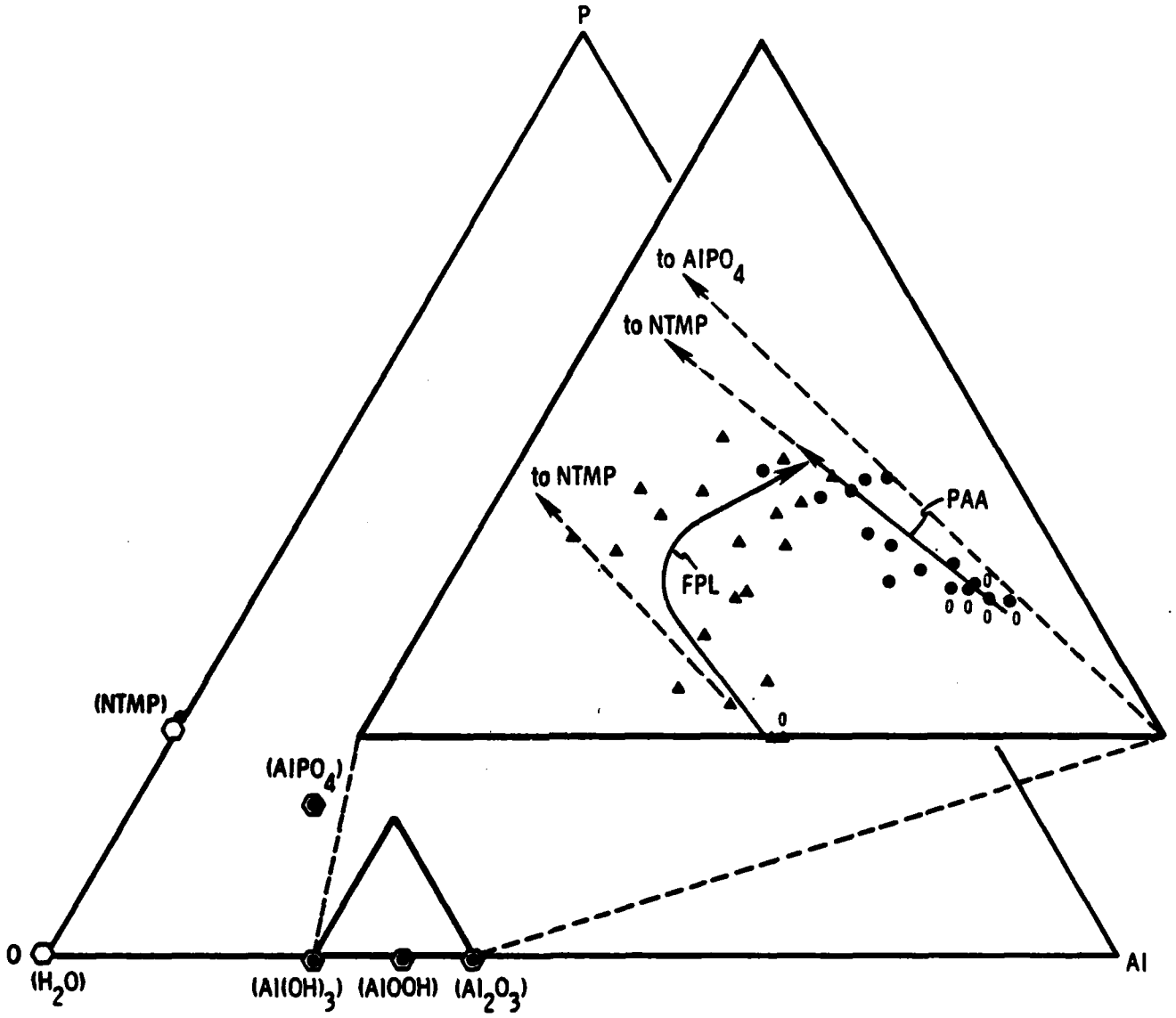

Figure 6. Al-P-O SED showing the surface composition of FPL-etched surfaces (triangles) and PAA-treated surfaces (circles) after immersion in solution of NTMP at various concentrations. Open hexagons are calculated compositions. Closed symbols are measured compositions. Compositions denoted by "0" represent surfaces not immersed in NTMP solutions.

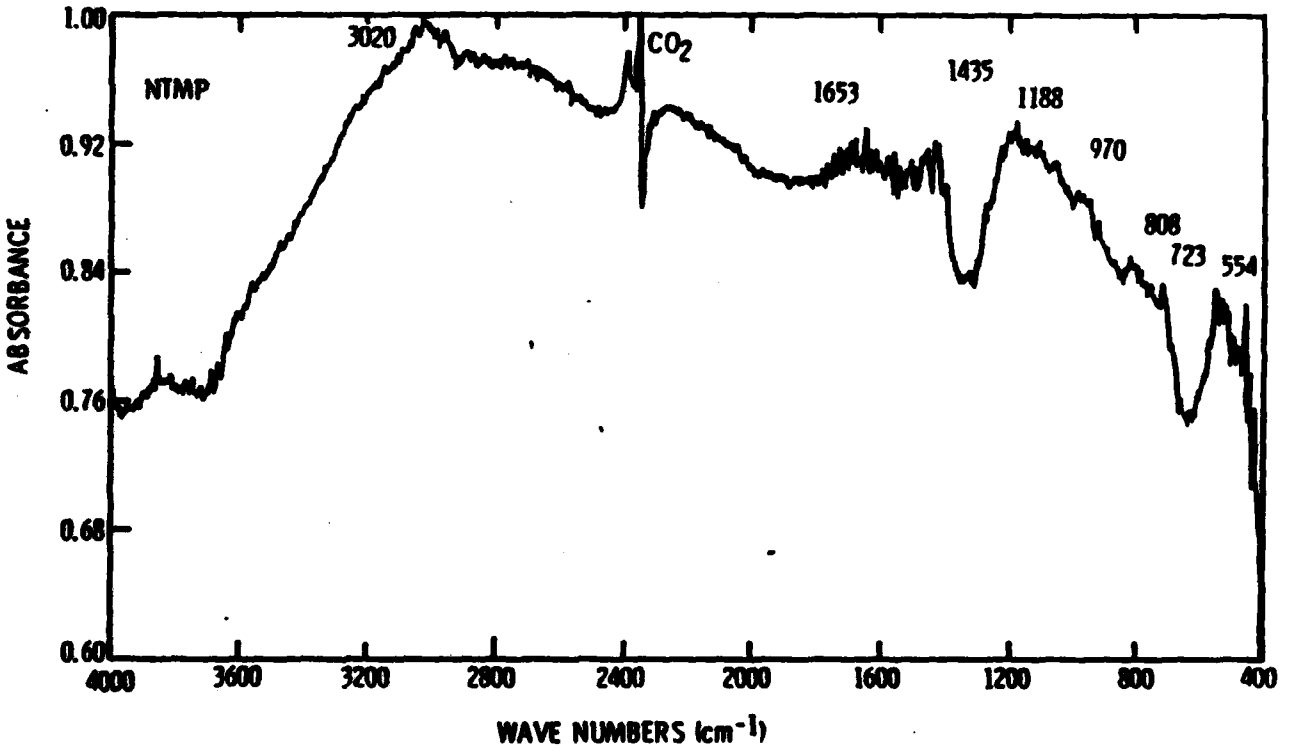

Figure 7. FTIR DRIFT spectrum of dried NTMP.

and determination of the probable bonding of NTMP to the aluminium surface was facilitated by studying the DRIFT spectrum of an Al-NTMP complex formed by reacting $Al(NO_3)_3$ with NTMP in a 2:1 molar ratio (Fig. 8 and Table 2). Significant changes in the P=O and P-O bonds (1200-700 cm^{-1}) are evident. The P=O bond for Al-NTMP is much sharper than that for NTMP, indicating a decrease of symmetry on the PO_3^{2-} group. Additionally, the P-O bond for Al-NTMP is shifted to lower wave-numbers, indicating the formation of an Al-O-P bond which is also detected at 956 cm^{-1}. By analogy, therefore, we can conclude that the NTMP molecule adsorbs to an aluminium oxide surface via the P-OH groups of the phosphonic acid.

B. HYDRATION

The hydration of NTMP-treated FPL surfaces in 100% relative humidity at 50°C has also been investigated by XPS and SBD's. As shown in Fig. 9, the hydration path proceeds from an NTMP covered Al_2O_3 surface to a boehmite [AlOOH] surface (line "a") and then to one of bayerite [$Al(OH)_3$]. Although considerable scatter occurs from coupon to coupon so that the degree of hydration at any one exposure time varies from run to run and even from one side of the coupon to the other, the general trend is clear. Additional variation is caused by physisorbed water,[10] represented by line "b", which was calculated by the addition of approximately one monolayer of water to surface compositions along line "a." Surfaces with compositions along line "b" lost this physisorbed water upon exposure to the dehydrating ultrahigh vacuum (UHV) for several days so that their final composition was near line "a." Finally, Auger depth profiles of

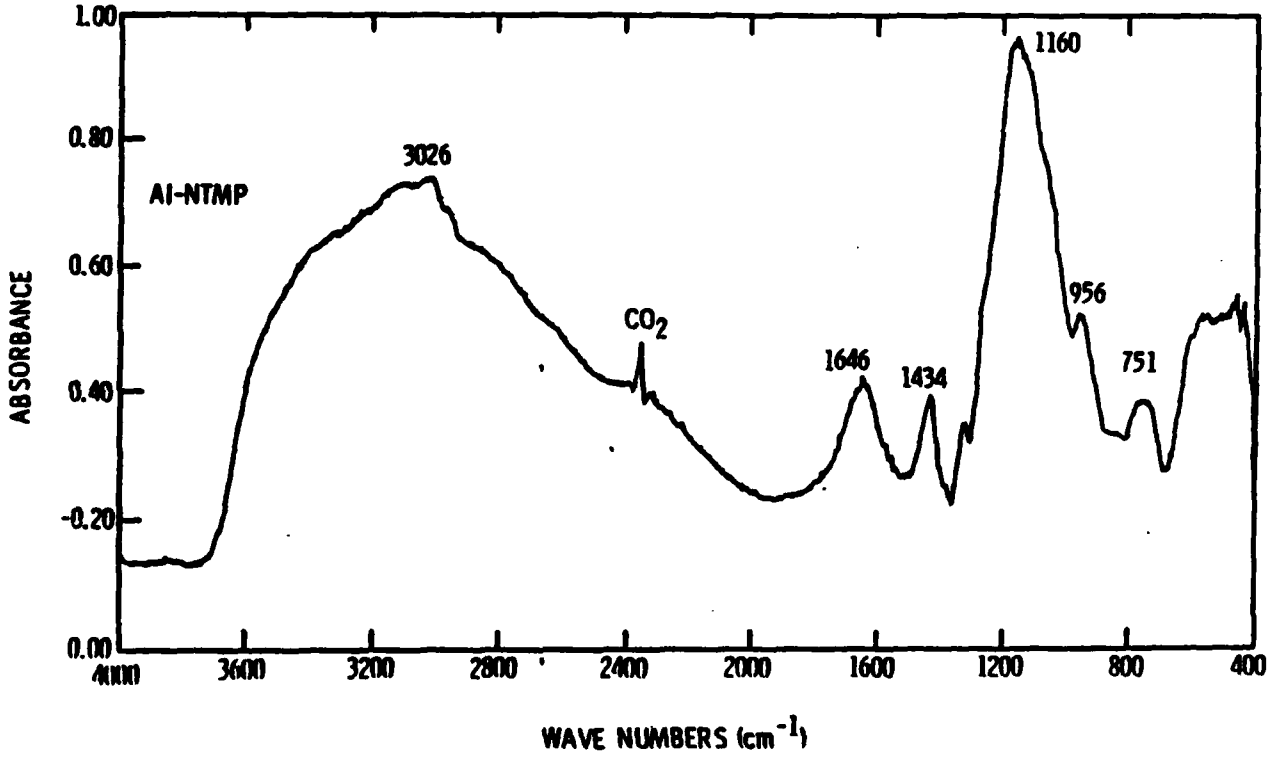

Figure 8. FTIR DRIFT spectrum of the Al-NTMP complex.

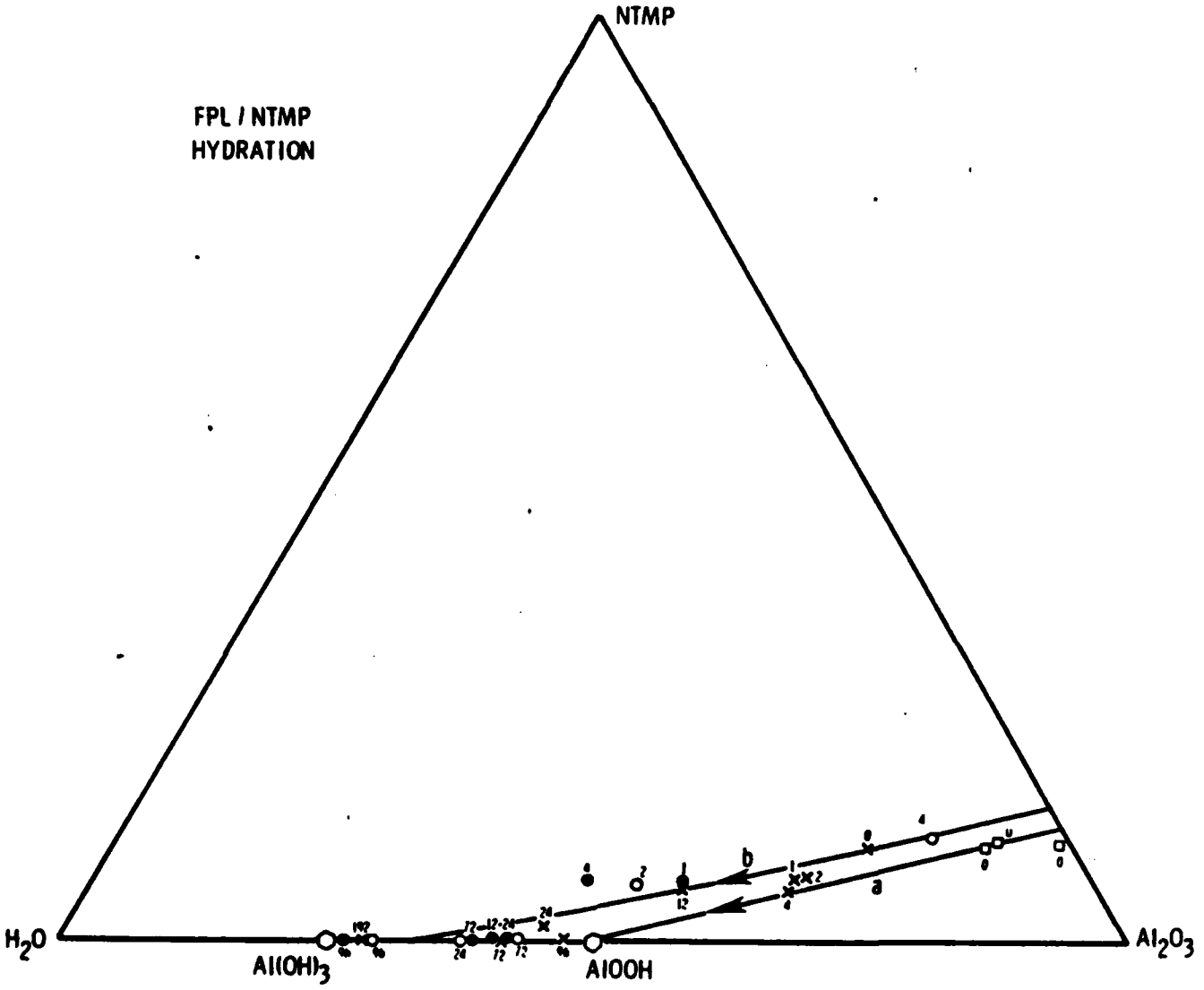

Figure 9. Al_2O_3-NTMP-H_2O SBD showing the evolution of the surface composition of FPL-etched surfaces treated with saturation coverages of NTMP, as a function of exposure time in 100% relative humidity at 50°C. The different symbols represent different experimental runs; the numbers are the exposure time in hours.

several samples revealed no subsurface concentration of phosphorus for coupons without surface phosphorus.

Similar hydration behavior is also observed for FPL surfaces treated with (n Bu) NBMP (Fig. 10). The surface again evolves from Al_2O_3 with a monolayer of inhibitor directly to AlOOH and then to $Al(OH)_3$.

C. WEDGE TESTS

Wedge tests were performed with FPL adherends treated with NTMP and several varients: AMP, i.e., replacing two of the methylene phosphonic groups with hydrogen atoms; MP, i.e., replacing the amino group of AMP with a hydrogen atom; and (n Bu) NBMP, i.e., replacing one methylene phosphonic group of NTMP with a linear hydrocarbon chain. From the results shown in Fig. 11, it is clear that the MP-treated specimens are worse than the untreated FPL samples or any of the adherends treated with other compounds. Each of these samples are, in turn, better than the control, with AMP achieving a smaller increase in long-term bond durability than either NTMP or (n Bu) NBMP.

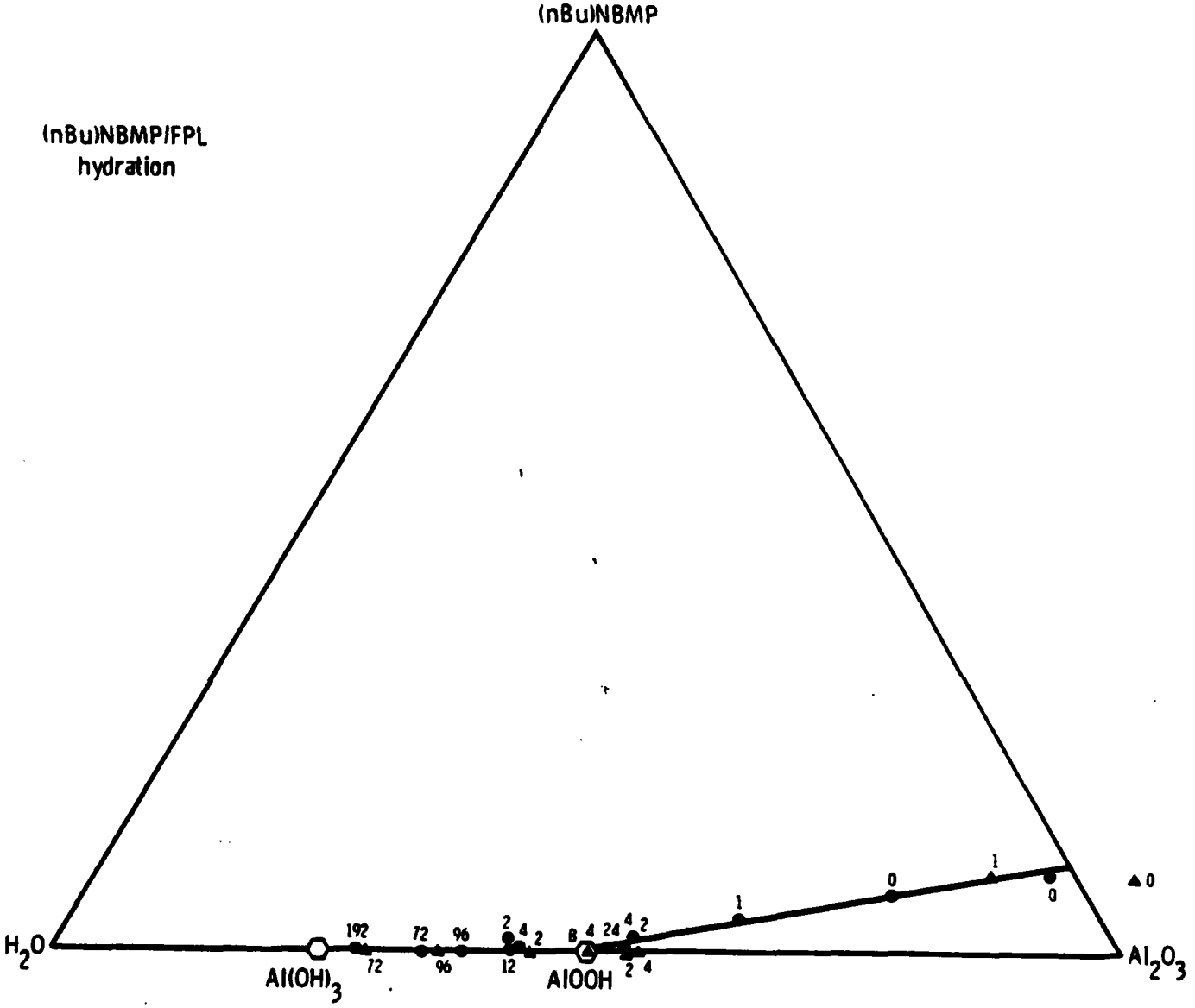

Figure 10. Al_2O_3-(n Bu) NBMP-H_2O SBD showing the evolution of the surface composition of FPL-etched surfaces treated with (n Bu) NBMP, as a function of exposure time on the humidity chamber. The different symbols represent different experimental runs; the numbers are the exposure time in hours.

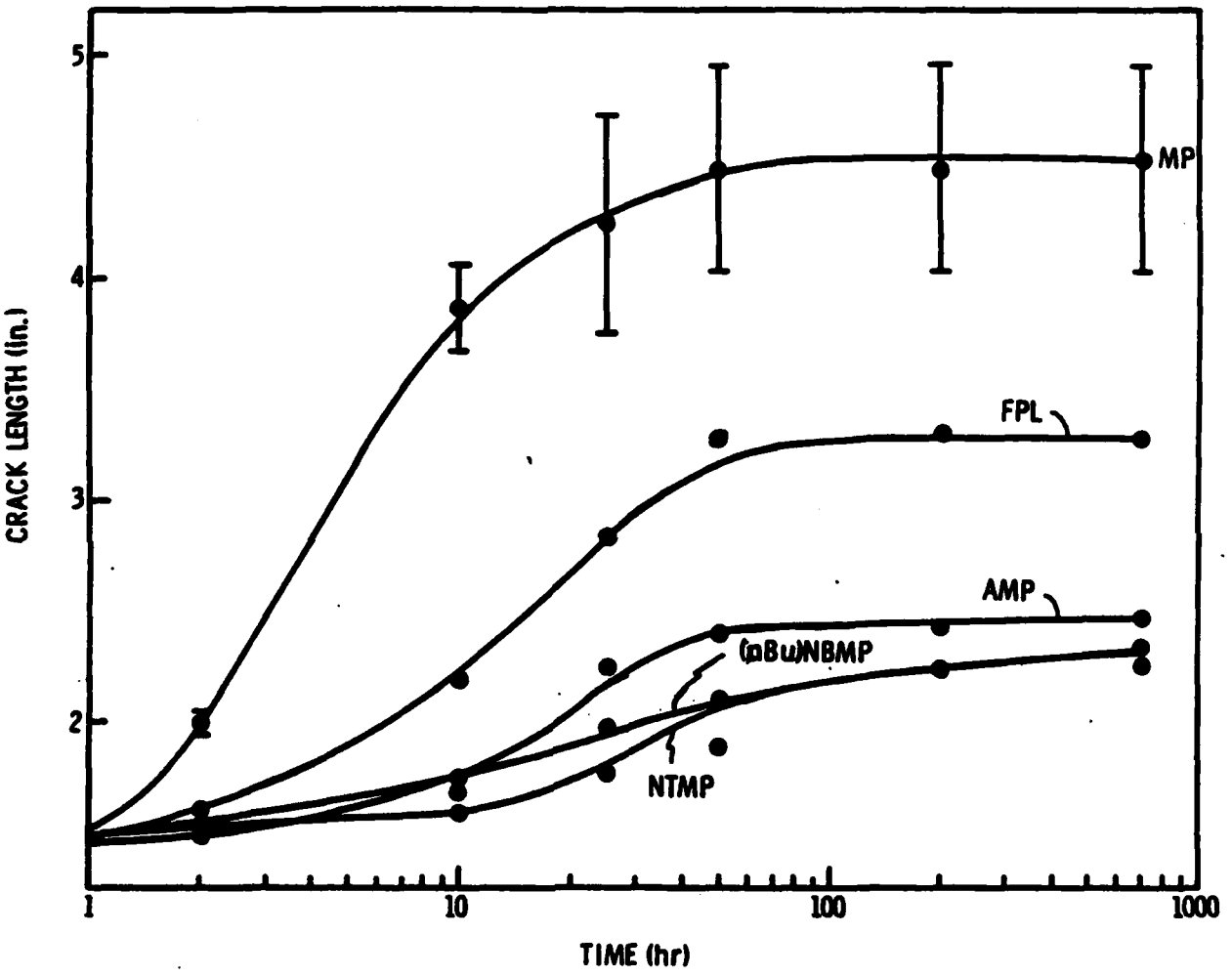

Figure 11. Wedge-test results (crack length as a function of time) for FPL adherends treated in solutions of MP, AMP, (n Bu) NBMP, and NTMP and for untreated FPL adherends.

IV. DISCUSSION

A. ADSORPTION

The adsorption of each of the three amino phosphonates studied proceeds by the displacement of the physisorbed water always present on the FPL surface. (This water can also be removed by storing the coupon in UHV for several days. The surface, however, regains the water upon exposure to the normal humid atmosphere.) For NTMP and (n Bu) NBMP this reaction, at room temperature, continues until all the physisorbed water has been replaced on the surface and approximately one monolayer of inhibitor is chemisorbed on Al_2O_3. Although less data exist for AMP, it appears that this inhibitor is less efficient at removing all the physisorbed water so that some water remains even at the highest AMP coverages achieved at room temperature. Since the presence of physisorbed water was identified as the first step in the hydration of PAA surfaces,[10] and will be shown to be a precursor of the hydration of NTMP-treated FPL surfaces later in this report, its incomplete removal upon AMP adsorption may help explain the poorer wedge test results for AMP-treated adherends. Different bonding between the inhibitor and the adhesive may also be a factor.

When closely examined the adsorption data of NTMP on FPL reveal further details of the adsorption competition between NTMP and H_2O, as indicated in Fig. 1 which shows the adsorption isotherm to be concave down. They are more clearly illustrated in Figs. 5 and 6, which show the isotherm as a two-part curve - at first proceeding in the general direction

of NTMP, but then heading more or less away from the H_2O vertex. We interpret these results as suggesting that the NTMP initially, i.e., at very low solution concentrations, adsorbs with only one leg bonded to the surface. Consequently the inhibitor coverage, as determined by the amount of P on the surface, increases faster than the water concentration on the surface decreases. Subsequently, i.e., at higher concentrations, the NTMP is able to compete more successfully with the water for adsorption sites and the other legs of the NTMP molecule become bonded to the surface, thus displacing water without a significant increase in the inhibitor coverage.

A two-step process, similar to that for NTMP on FPL but less pronounced, would be expected for the adsorption onto FPL of (n Bu) NBMP, a single-step process would be expected for AMP, however, since it has only one methylene phosphonic acid group. The SBD's of Figs. 3, 4, and 5 support this hypothesis. Although the data for (n Bu) NBMP and AMP are more scattered than those for NTMP, Fig. 5 clearly shows only a slight curvature in the surface composition evolutionary path for AMP on FPL in contrast to the distinct two-step adsorption process for NTMP on FPL. Figures 4 and 5 also show that AMP is less efficient at removing all the physisorbed water so that some water remains even at the highest AMP coverages achieved at room temperature. This presence of residual water is consistent with the lower phosphorus content on the surface at saturation. Our model of adsorption suggests one phosphorus atom for every two water molecules removed from the surface (assuming that all the inhibitor's POH groups bond to the Al_2O_3). Since the AMP-treated surface has a

significantly lower P/Al ratio, less water would have been displaced from the surface.

In contrast, the adsorption of NTMP onto PAA surfaces causes the surface composition to evolve directly toward NTMP (Fig. 6), indicating a simple adsorption process. This is expected, however, because initially there is little water on the PAA surface to displace.

The saturation coverage of phosphorus-containing groups is very similar between NTMP on PAA and NTMP on FPL as reported earlier.[6,7] From these data we can not differentiate between NTMP adsorbing only on unoccupied active sites and NTMP displacing the phosphate incorporated onto the surface during anodization[10] in a competitive adsorption mechanism. We can rule out a displacement of all of the initial phosphate however, by comparing typical N concentrations on the NTMP/PAA and the NTMP/FPL surfaces, ~ 1.5% and ~ 2.5-3.0%, respectively. Because there is considerably less N relative to P on the PAA-treated surfaces, it is clear that the NTMP has either simply adsorbed on unoccupied active sites, or displaced only a fraction of the phosphate initially present on the PAA surface. In either case, the adsorption of NTMP on PAA further improves the hydration resistance and the long-term bond durability.[6]

B. HYDRATION AND WEDGE TESTS

The behavior of the surface composition during the hydration of NTMP-treated FPL surfaces (Fig. 9) is very similar to that observed during the hydration of PAA surfaces.[10] First, a reversible physisorption of water occurs. Then the surface hydrates to boehmite. Finally, bayerite

crystallites grow on top of the boehmite. It is this hydration to boehmite, during which adhesive bonds fail, that the inhibitor is effective in slowing. In fact, the linear evolutionary path of the surface composition to boehmite and the absence of any subsurface phosphorus in the hydrated samples indicate that hydration only occurs as the NTMP dissolves from the surface. That is, the limiting step in the hydration of these surfaces is the dissolution of NTMP into the condensed water vapor.

These findings, which have been generalized to include the corrosion of NTMP-treated steel samples[13] as well as the hydration of PAA surfaces,[10] suggest several properties of an ideal inhibitor: 1) the inhibitor should occupy all the active sites on the surface, 2) the inhibitor should bond strongly to the surface, and 3) the inhibitor - aluminum complex should be insoluble in water.

An additional property, that the inhibitor must be compatible with the primer/adhesive system used, can be deduced from the wedge tests of Fig. 11 which show extremely poor performance by MP-treated adherends, the wedge tests of reference 9 which showed poor performance of phosphoric-acid-immersed adherends, and the T-peel tests of reference 6 which showed poor initial bond strength of NTMP-treated adherends bonded with a nitril phenolic adhesive. In the first two cases, the P=O bond, that is oriented away from the inhibited surface, either interfered with the curing of the epoxy adhesive at the surface or passivated the adherend surface and prevented the formation of adhesive-oxide or adhesive-inhibitor chemical bonds. Either possibility results in degraded bond durability even-though the inhibited oxide may be resistant to hydration. Similarly the

NTMP is believed to have prevented the nitrile phenolic adhesive from completely curing at the surface, resulting in poor bond strength.

Based on these four criteria we are currently modifying the NTMP molecule in attempts to improve its inhibition efficiency. The first of our new compounds is (n Bu) NBMP, where one of the methylene phosphonic acid groups is replaced with a linear hydrocarbon chain to decrease the aqueous solubility of the inhibitor-aluminum complex and to increase the miscibility with the adhesive. At the same time, however, this action has the adverse effect of decreasing the number of P-O-Al bonds to the surface.

Initial hydration studies (incubation times in excess of 120 minutes for coupons treated with each inhibitor) and wedge tests (Fig. 11) suggest that these two effects may balance, resulting in little net difference between the efficiency of NTMP and (n Bu) NBMP to inhibit hydration and to improve bond durability. Additional tests are currently underway to examine further the effectiveness of these inhibitors and others, including (ter-butyl) nitrilobis methylene phosphonic acid, a structural isomer of (n Bu) NBMP, and ethylene diamine tetramethylene phosphonic acid, a four-legged variant of NTMP.

V. SUMMARY

We have investigated the mechanisms by which nitrilotris methylene phosphonic acid (NTMP) and related compounds adsorb onto oxidized aluminum surfaces, inhibit the hydration of this oxide, and increase the durability of adhesive bonds formed with treated panels. Our results indicate that: 1) NTMP adsorbs via P-O-Al bonds; 2) water initially adsorbed onto the FPL surface is displaced by the NTMP; and 3) hydration of NTMP-treated FPL surfaces occurs in three stages -- i) a reversible physisorption of water, ii) the slow dissolution of NTMP followed by the rapid hydration of the freshly exposed Al_2O_3 to AlOOH, and iii) the further hydration of the surface to $Al(OH)_3$. Additionally, by comparing the behavior of coupons treated with different inhibitors, we have identified four properties of the ideal inhibitor: 1) the inhibitor should occupy all the active sites on the surface, 2) the inhibitor should bond strongly to the surface, 3) the inhibitor-aluminum oxide complex should be insoluble in water, and 4) the inhibitor should be compatible with the primer/adhesive system.

VI. REFERENCES

1. H.W. Eichner and W.E. Schowalter, Forest Products Laboratory Report No. 1813, Madison, WI, 1950.

2. G.S. Kabayaski and D.J. Donnelly, Boeing Corporation Report No. D6-41517, Seattle, WA, February 1974.

3. J.D. Venables, D.K. McNamara, J.M. Chen, and T.S. Sun, Appl. Surf. Sci. 3, 88 (1979).

4. D.J. Packham, in Adhesion Aspects of Polymeric Coatings, ed., K.L. Mittal, Plenum, New York, 1983, and the references therein.

5. J.D. Venables, D.K. McNamara, J.M. Chen, B.M. Ditchek, T.I. Morgenthaler, and T.S. Sun, in Proc. 12th Natl. SAMPE Techn. Conf., Seattle, WA, 1980, p. 909.

6. D.A. Hardwick, J.S. Ahearn, and J.D. Venables, MML TR 82-23c, End-of-Second-Year Report under ONR Contract N00014-80-C-0718, Martin Marietta Laboratories, Baltimore, MD.

7. D.A. Hardwick, J.S. Ahearn, and J.D. Venables, accepted by J. Mater. Sci.

8. J.S. Ahearn, G.D. Davis, T.S. Sun, and J.D. Venables in Adhesion Aspects of Polymeric Coatings, ed., K.L. Mittal, Plenum, New York, 1983.

9. J.S. Ahearn, G.D. Davis, A.I. Desai, and J.D. Venables, MML TR 81-46c, End-of-First-Year Report under ONR Contract N00014-80-C-0718, Martin Marietta Laboratories, Baltimore, MD.

10. G.D. Davis, T.S. Sun, J.S. Ahearn, and J.D. Venables, J. Mater. Sci. 17, 1807 (1982).

11. G.D. Davis, S.P. Buchner, W.A. Beck, and N.E. Byer, Appl. Surf. Sci. 15, 238 (1983).

12. A.I. Plaza, PhD Thesis, University of Maryland, Jan. 1976 (unpublished).

13. G.D. Davis, J.S. Ahearn, and J.D. Venables, accepted by J. Vac. Sci. Technol.

A Report

Application of IETS to the Study of Hydration Inhibitors on Aluminum Oxide

Prepared

for

Martin Marietta Corporation

Office of Naval Research

and

Army Research Office

for work performed under Subcontract No.

MML-MSS-83-02

as part of Contract No.

N00014-80-C-0718

Prepared

by

Henry W. White, P.I.

Physics Department

University of Missouri-Columbia

Columbia, MO 65211

August, 1983

Application of IETS to the Study of Hydration

Inhibitors on Aluminum Oxide

Table of Contents

List of Figures

List of Tables

I. Introduction

A. Goals and Approach

The goal of the current work is to use Inelastic Electron Tunneling Spectroscopy (IETS) to investigate the orientation and bonding of several hydration inhibitors on aluminum oxide. This information will be combined with measurements at Martin Marietta Laboratories to determine mechanisms whereby these molecules can inhibit the hydration of aluminum oxide in the presence of moisture. In this report we discuss results obtained for the following phosphonate-type molecules:

Phosphonic Acid	PA
Methylphosphonic Acid	MPA
Hydroxymethylphosphonic Acid	HPA
Nitrotrismethylphosphonic Acid	NTMP

In the course of developing a model for tunneling intensities to apply to the IETS spectra for MPA we did extensive model development and model calculations for thiourea and urea which served as test-case molecules. This approach has been fruitful.

B. Overview of Results: This report is organized as follows:

In Section II we discuss IETS spectra for PA, HMP, and NTMP. Mode assignments have been made for the main peaks in each of the spectra, and differences and simularities are discussed. The locations and shapes of the P=O stretch mode and the P-O-(H) modes are discussed in particular.

In Section III we summarize the main features of a model for calculating IETS peak intensities. This model, which we have termed the floating valence model, contains several significant improvements over other models. Intensities calculated for various orientations of thiourea have been critically compared with experimental values to determine the orientation of the adsorbed species. These results are now being evaluated. The model is

clearly the most sophisticated and accurate of the existing tractable models, and it has been successfully applied to a complex molecule having several atom types. In our summary of Section II we evaluate the feasibility of applying this model to the inhibitor molecules in this study.

In Section III some of the methods developed for use in the floating valence model have been used to determine molecular structure and to calculate the charges associated with each of the atoms in the molecules PA, MPA, and HMP.

The charges are obtained by a potential derived (PD) technique, and these are shown to be considerably more accurate and reliable than those obtained from Mullikan population analysis.

Section V is a statement of the main conclusions from our work under this project.

II. IETS Spectra for Adsorbed Inhibitors

A. Experimental Techniques

The IETS measurements were made on tunnel junctions prepared on insulating ceramic substrates. An aluminum electrode approximately 1000 Å thick was evaporated onto the substrate at 10^{-7} to 10^{-8} Torr. An oxide layer was grown on the aluminum and then doped with a water based solution of the inhibitor or other molecule to be studied. This doping process was done outside the vacuum chamber. The doped substrate was then returned to the vacuum chamber and a top metal electrode of Pb was evaporated to complete the junction. Electrical leads were attached, the resistances were measured, and those junctions with good electrical characteristics were immersed in liquid helium for IETS measurements.

One of the problems associated with the early stages of this work was the inability to obtain a significant yield of junctions which had resistances in the appropriate range, were stable, and

had good signal to noise characteristics. Several approaches were used to solve this problem. This problem has also occurred when molecules containing chlorine atoms are used as dopants.

We can now prepare junctions with much improved signal to noise ratios by a two-step oxidation process which combines a DC glow discharge in oxygen followed by growth at elevated temperatures. Good yields have been obtained for molecules as large as NTMP.

B. IETS Spectra

This section contains spectra obtained for PA, HMP, and NTMP. For each inhibitor the observed frequencies and mode assisments are listed in a table. These assignments and spectra features are then discussed in each section.

Spectra taken on junctions doped with MPA indicated that no MPA had remained on the oxide surface.

1. PA

IETS spectra for PA obtained on a junction doped with 0.3% solution of PA in water are shown in Figures 1(a) and 1(b). The range and measurement conditions are different for the two scans. Figure 1(a) shows the lower frequency modes; whereas, Figure 1(b) shows more of the over-all spectral features including the higher frequency C-H and O-H stretch regions.

The peak locations in the spectra have been labeled in units of cm^{-1} and listed in Table I. The mode assignments for each of those peaks are also listed. These assignments are compared with the spectra HMP and NTMP in Section 5 below.

2. HMP

The HMP spectra shown in Figure 2(a) and 2(b) were taken on junctions doped with a solution with a concentration of 10 mg of HMP per ml of water. The peak positions and mode assignments are given in Table II. They are compared with the features of PA and NTMP in Section 5.

3. NTMP

The IETS spectra for a 0.1% solution of NTMP is shown in Figure 3(a) and 3(b). Table III lists peak locations and assignments, with further comparison in Section 5.

C. Results for MPA

Junctions doped by the same procedures as those used for the other molecules indicated that little, if any, MPA remained on the oxide layer. The general appearance of the oxide layer to the naked eye and also under a low power microscope suggested that the MPA did not react with the oxide layer in the manner in which the other molecules did. Our plans regarding further studies on MPA are unclear at this point. One of the original goals of this study was to compare calculated and experimental intensities for MPA to determine the orientation of the adsorbed molecule. These experimental results, when coupled with the lack of a complete molecular vibrational analysis on MPA, indicate that this molecule is not a suitable choice for this study at this time.

D. Discussion of IETS spectra

An aluminum phonon near 320 cm^{-1}, an aluminum oxide phonon near 945 cm^{-1} and a 2x aluminum phonon occur in each of the spectra and arise from features of the junction electrodes. They will not be discussed further.

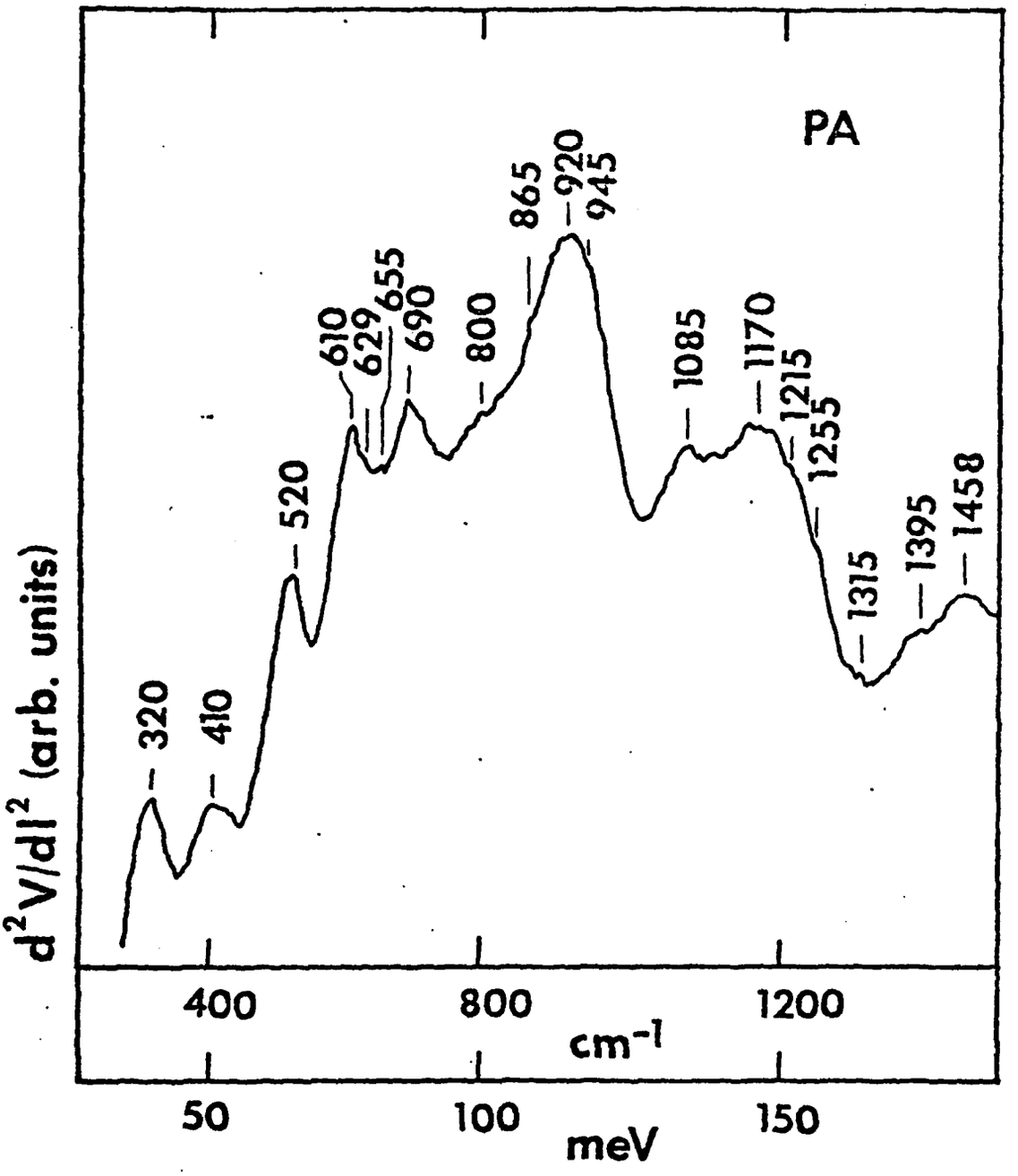

Fig. 1(a). IETS spectrum from 300 to 1500 cm^{-1} for a 0.3% solution of PA in water.

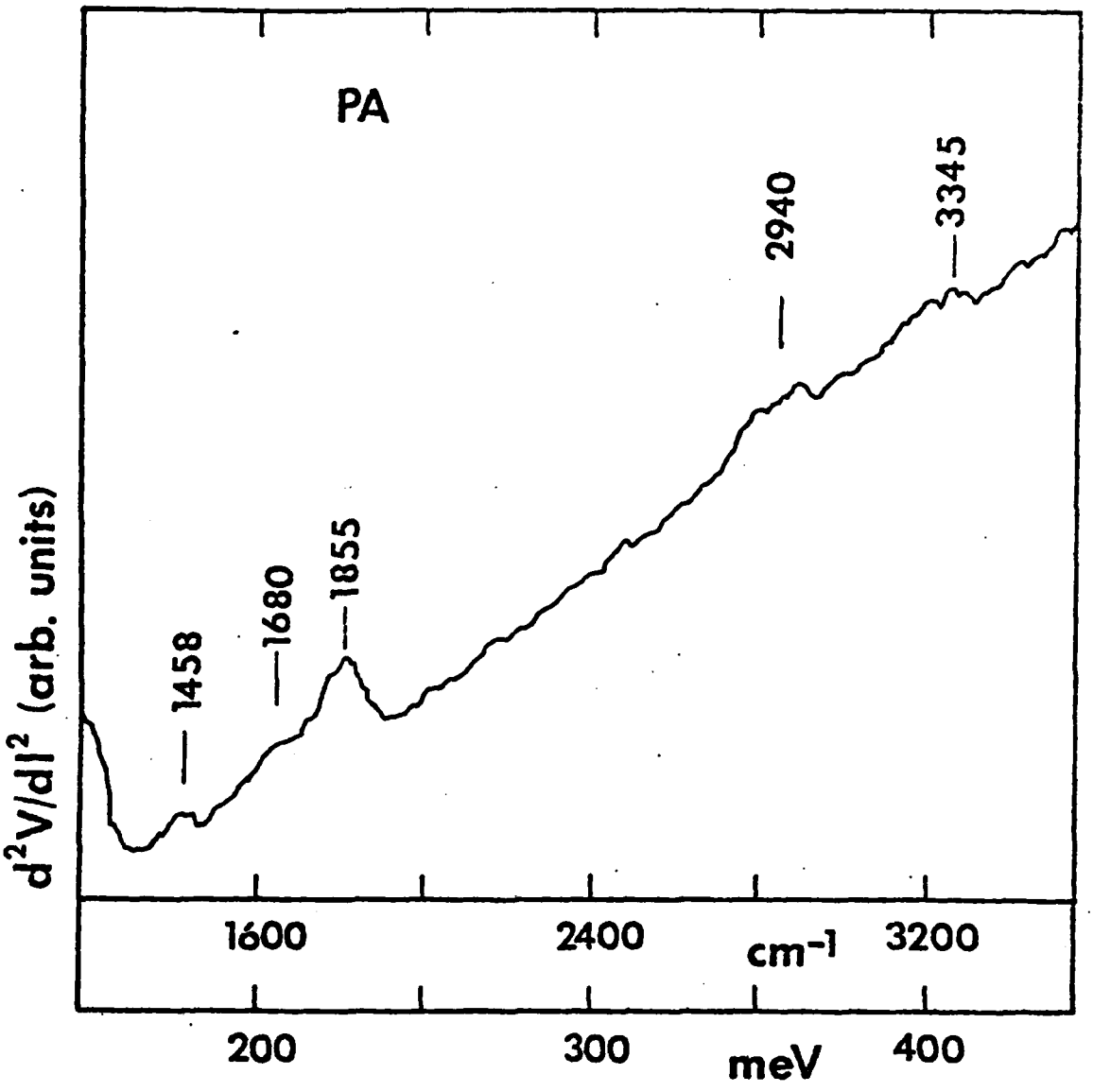

Fig. 1(b). IETS spectrum from 1200 to 3600 cm^{-1} for a 0.3% solution of PA in water.

Table I. Vibrational mode frequencies and assignments for PA adsorbed on aluminum oxide as measured by IETS.

Frequency (cm^{-1})	Relative Strength[a]	Group Assignment
320	vs	Al phonon
410	s	
520	s	PO_3 in-plane, or P=O defm
610	s	P-O defm
629	vw	
655	vw	
690	s	
800	w	
865	sh	
920	vs	
945	sh	Al oxide phonon
1085	m	P-O-(H) str
1170	b	P=O str
1215	w,sh	P=O str ?
1255	w,sh	
1315	vw	C-H (contamination)
1395	vw	C-H (contamination)
1458	m,b	C-H (contamination)
1700	m	
1680	w,b	
1855	s,b	2x Al oxide phonon
2940	w,b	C-H str (contamination)

a. w = weak, vw = very weak, m = medium, s = strong, vs = very strong, b = broad, sh = shoulder.

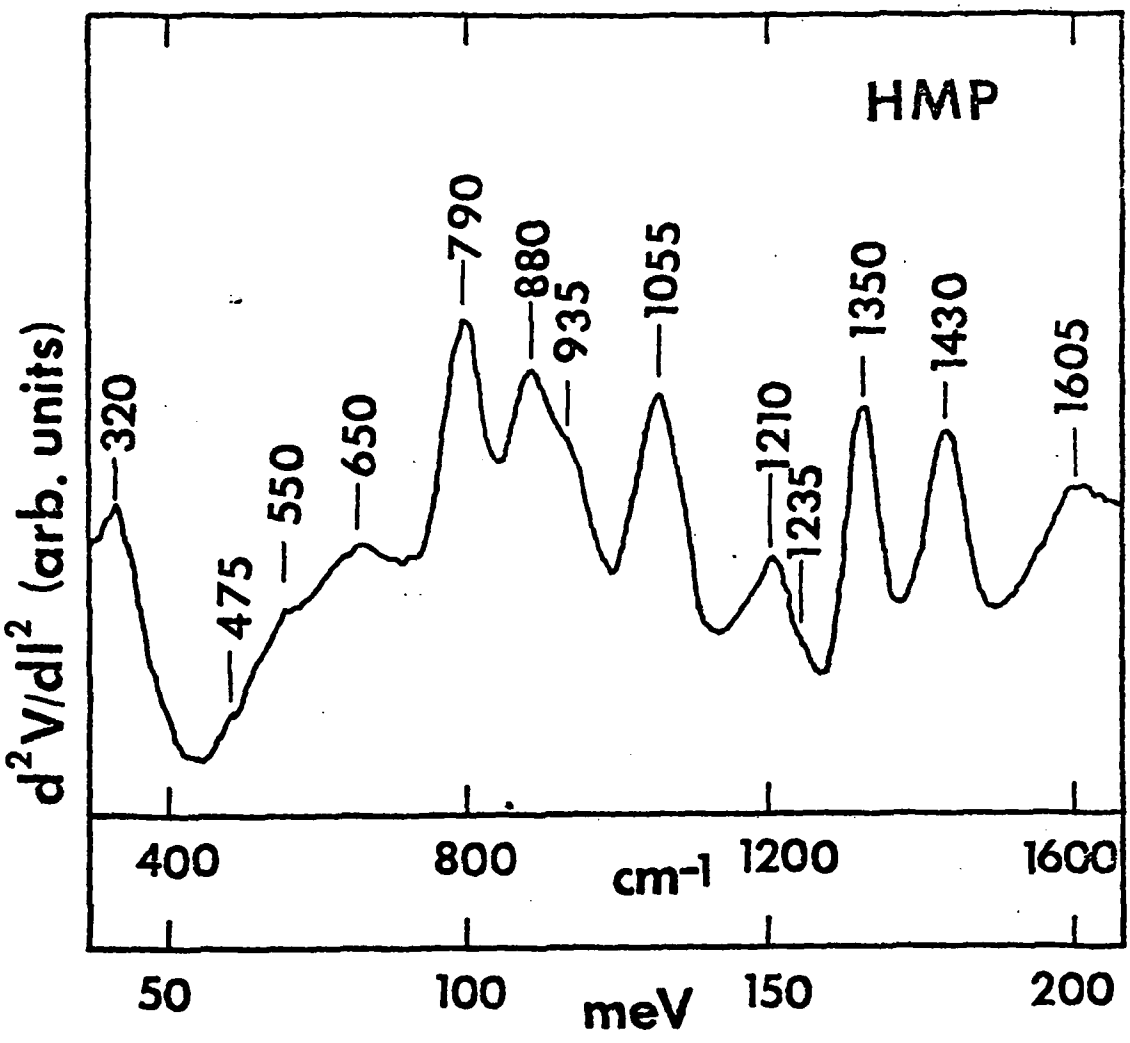

Fig. 2(a). IETS spectrum from 300 to 1650 for a 1% solution of HMP in water.

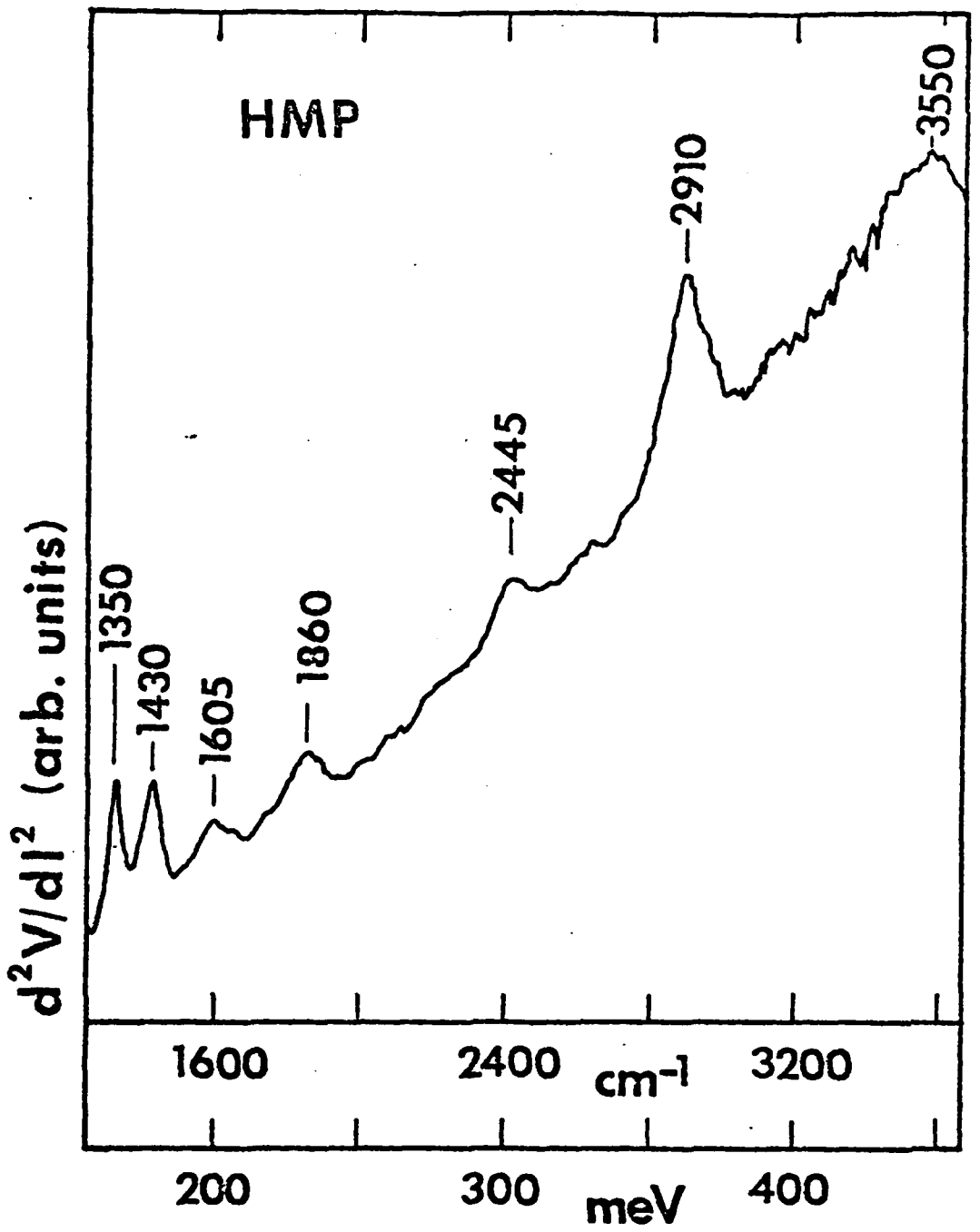

Fig. 2(b). IETS spectrum from 1300 to 3600 cm^{-1} for a 1% solution of HMP in water.

Table II. Vibrational mode frequencies and assignments for HMP adsorbed on aluminum oxide as measured by IETS.

Frequency (cm^{-1})	Relative Strength[a]	Group Assignment
320	vs	Al phonon
475	vw	PO_3 in-plane, or P=O defm
550	w	P-O or P=O defm
650	b	
790	vs	P-O str
880	vs	CH_2
935	sh	Al oxide phonon
1055	vs	P-O-(H) str
1210	vs	P=O str
1235	w,sh	O-H defm
1350	vs	CH_2 wag
1430	vs	CH_2 defm
1605	s,b	
1860	m,b	2x Al oxide phonon
2445	m,b	Fermi resonance ?
2910	vs,b	C-H str
3550	m,b	O-H str

a. w = weak, vw = very weak, m = medium, s = strong, vs = very strong, b = broad, sh = shoulder.

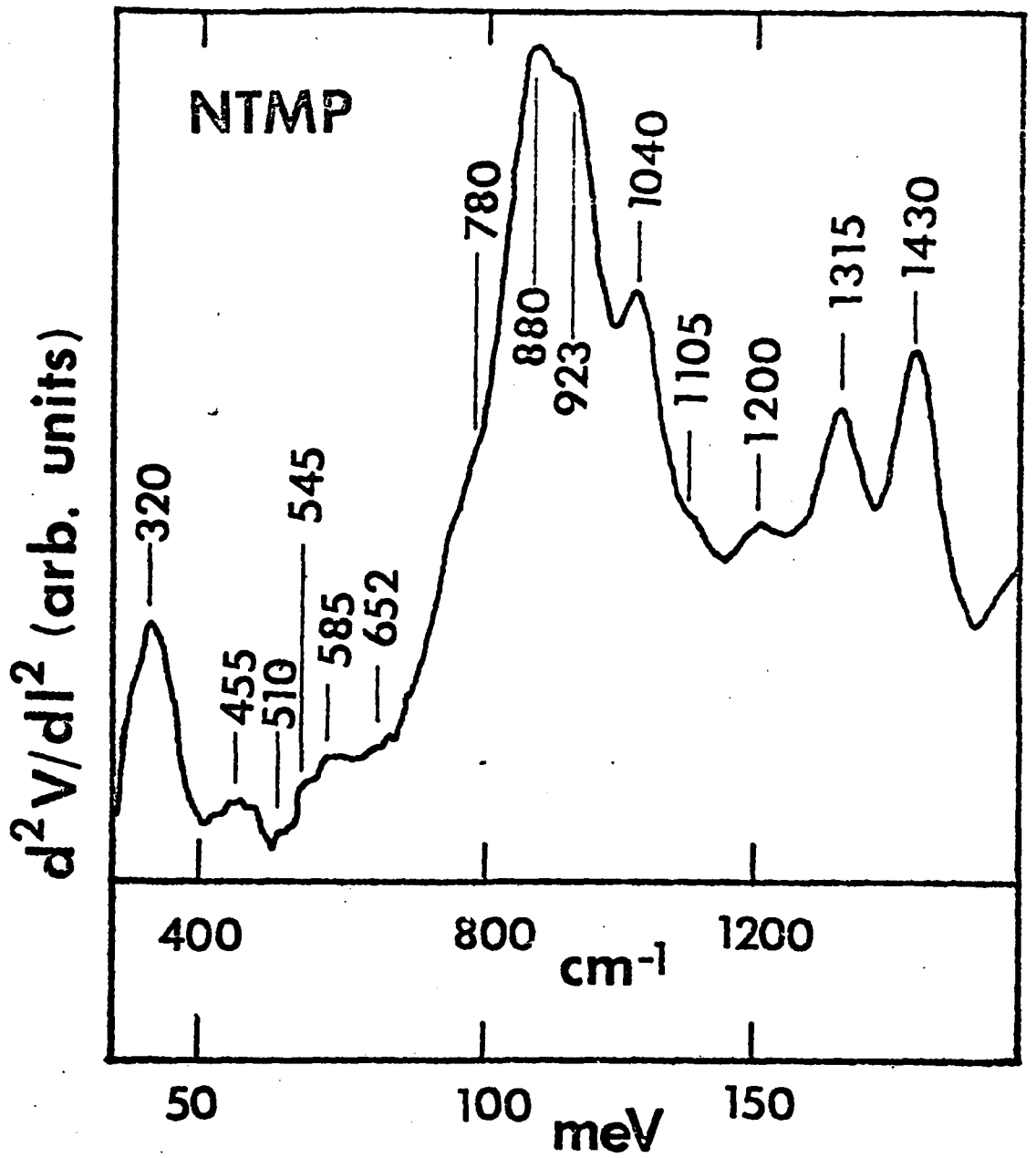

Fig. 3(a). IETS spectrum from 300 to 1600 cm^{-1} for a 0.1% solution of NTMP in water.

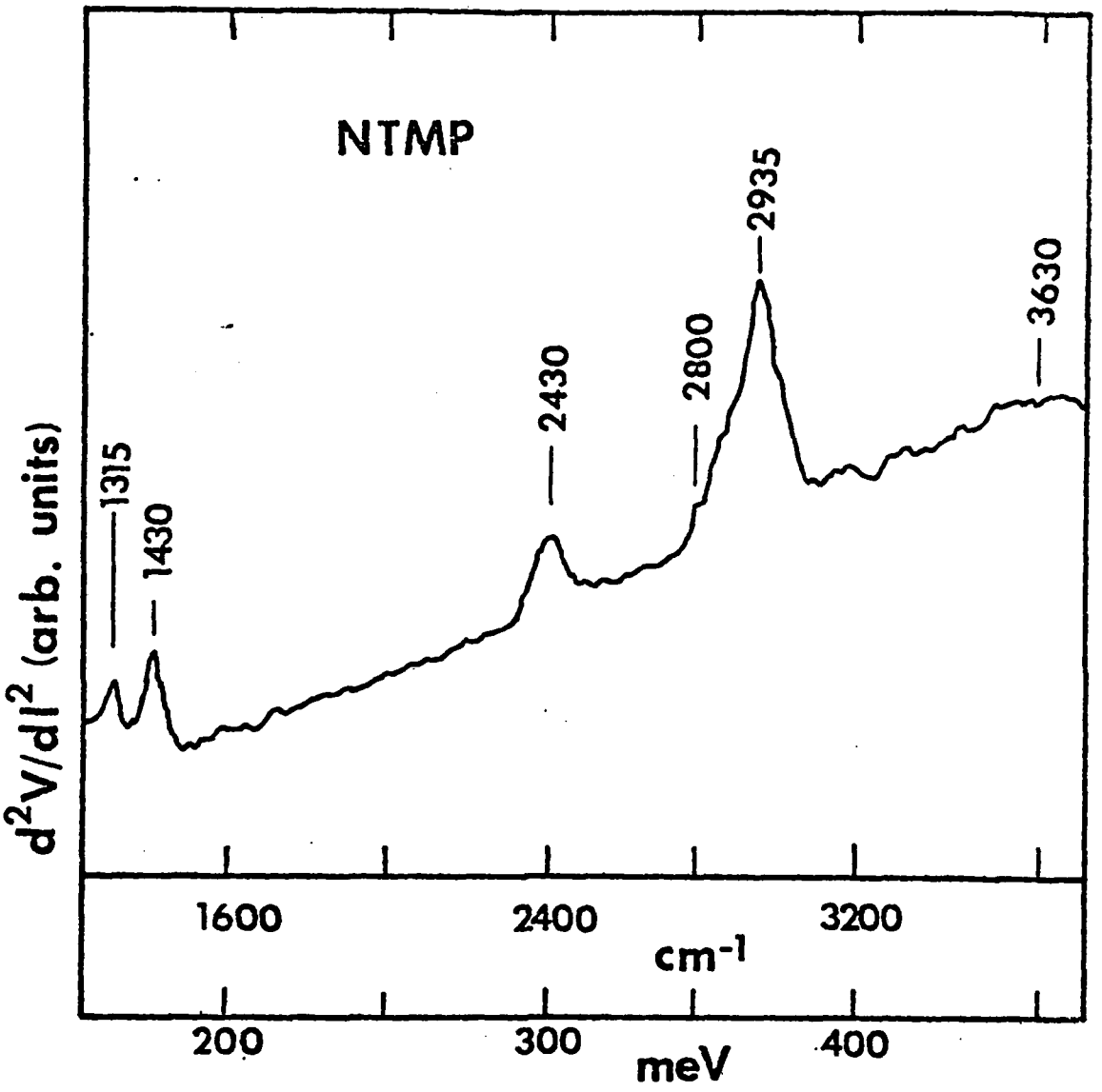

Fig. 3(b). IETS spectrum from 1200 to 3700 cm^{-1} for a 0.1% asolution of NTMP in water.

Table III. Vibrational mode frequencies and assignments for NTMP adsorbed on aluminum oxide as measured by IETS.

Frequency (cm^{-1})	Relative Strength[a]	Group Assignment
320	vs	Al phonon
455	b	PO_3, or P=O defm
510	vw	PO_3, or P=O defm
545	vw	P-O defm
585	b	P-O defm
652	vw	
780	s	P-C str
880	vs	CH_2
923	s,sh	Al oxide phonon
1040	vs	P-O-(H) str
1105	w,sh	
1200	b	P=O str
1315	vs	CH_2 wag
1430	vs	CH_2 defm
2430	vs	
2935	vs	C-H str

a. w = weak, vw = very weak, m = medium, s = strong, vs = very strong, b = broad, sh = shoulder.

We note the presence of weak bands at 475 and 455 in HMP and NTMP, respectively, whereas no peak occurs in PA in this region. Veken and Herman[1] assign a band as PO_3 in-plane motion which they observed near 480 cm^{-1} (VW) in IR and at 498 cm^{-1} (Sh/W) in Raman spectra of dibasic methylphosphonic acid in water. The PO_3 in-plane assignment for PA near 520 cm^{-1} is probably a PO_3 in-plane mode, but with different character.

Thomas and Chittenden[2] give a possible alternative description to these peaks. They describe a weak, diffuse peak near 500 cm^{-1} which they associate with P-O (OH) groups. Since the peaks are weak and can evidently be lost in some spectra they cannot be considered significant for these studies at this time.

The 545 and 585 cm^{-1} peaks in NTMP, even though weak and broad, are of interest since the FT-IR results of NTMP adsorbed on aluminum oxide show very strong, well formed peaks at 547 and 585 cm^{-1}. The FT-IR spectrum of dried NTMP also shows a band near 554 cm^{-1} which has been assigned as P-O motion. The IETS HMP shows a weak peak at 550 cm^{-1} and it is possible that the PA spectrum has a shoulder near 550 cm^{-1} but the results are not conclusive. These peaks are assigned as P-O deformation modes by comparison with data by Veken and Herman[1] In Table I we indicate a tentative assignment of this P-O deformation mode for the 610 cm^{-1} peak in PA.

There are several peaks in the PA spectra whose assignment is very unclear. Their locations are 629 (VW), 655 (VW), 690 (S), 800 (W), 865 (Sh), and 920 (VS). We are especially interested in the assignments of the strong peaks at 690 and 920 cm^{-1}. No strong peaks occur in the 690 cm^{-1} region of either HMP or NTMP. There are strong peaks at 880 cm^{-1} in each; however, they are clearly associated with the CH_2 motion in HMP and NTMP. The strong peaks at 790 cm^{-1} in HMP and at 780 in NTMP can also be assigned to P-C stretch motion.[1]

Peaks near 1085 (M) in PA, at 1055 (VS) in HMP and at 1040 cm^{-1} (VS) in NTMP are undoubtedly P-O-(H) stretch motions which are known to occur near 1000 (± 100) cm^{-1} for molecules with these end groups. The FT-IR data for NTMP adsorbed on aluminum oxide has a very strong, broad band near 1050 cm^{-1}, and the Al-NTMP complex has a peak near 1160 cm^{-1}, both of which could have P=O stretch contributions. We note that C-O stretch and out-of-plane C-H bend modes also occur near 1050 cm^{-1} in many compounds and could contribute to the peaks observed in all of these spectra since these contaminates are so prevalent.

We have assigned the peaks at 1210 (VS) in HMP and at 1200 (b) in NTMP as P=O stretch in accordance with many literature discussions of the phosphoryl frequency. According to Thomas and Chittenden[3] it sometimes occurs as a doublet and, as a result, can appear as such, or as a broad peak. In their extensive analyses of P=O stretch frequency shifts as a function of attached groups to phosphorus they found that the mean value was sufficient to provide agreement with other data. In PA a broad peak does occur at 1170 cm^{-1} which was assigned as P=O stretch. A weak shoulder at 1215 cm^{-1} was tentatively assigned as P=O stretch for lack of reasonable alternatives. The 1235 cm^{-1} peak in HMP is in the region expected for O-H deformations.

The location of the 1200 cm^{-1} P=O stretch peak in the IETS spectrum of NTMP should be compared with the value of 1256 cm^{-1} for the location of a peak as determined by FT-IR of NTMP adsorbed on aluminum oxide. The FT-IR of dried NTMP has a peak near 1188 cm^{-1}, and the Al-NTMP complex shows a strong peak near 1160 cm^{-1}.

The 1350 (VS) and 1430 (VS) peaks in HMP and the 1315 (VS) and 1430 (VS) peaks in NTMP were assigned as CH Wag and C-H deformation modes, respectively. Veken and Herman[1] found CH Wag and deformation modes at 1305 and 1430 cm^{-1} in dibasic $CH_3PO_3^{2-}$. The very weak peaks at 1315, 1395, and 1458 cm^{-1} in PA are likely to be due to CH contamination as suggested by the structure near 2940 cm^{-1} in PA (C-H stretch).

The very strong C-H stretch modes at near 2910 cm^{-1} in HMP and near

2935 cm^{-1} in NTMP are as expected for molecules containing aliphatic CH bonds (i.e., below 3000 cm^{-1} in almost all cases).

The medium intensity, broad band near 3550 cm^{-1} in HMP is easily assigned as O-H stretch.

There are interesting IETS peaks near 2445 cm^{-1} in HMP and 2430 cm^{-1} in NTMP which do not occur in PA. Although the nature of the modes is not clear, the fact that each is so strong, and occurs in a region where no strong peaks are expected suggests that they are due to a Fermi resonance (overtone or combination occurring near a fundamental of the same symmetry type). In this case the fundamental could be associated with an OH stretch mode since these can extend to much lower frequencies than 3550 cm^{-1} for phosphonic acid groups as discussed by Thomas and Chittenden[2].

The general features associated with the IETS spectra for PA, HMP, and NTMP are reasonable and consistent with what might be expected; yet, they show variations in the locations and appearance of certain modes. Of particular interest to this work is the behavior of the P=O stretch and of the P-O-(H) stretch vibrations. In Section IV of this report we show calculated values for the atomic charges associated with each atom site in PA, MPA, and HMP. We are interested in correlating features in the IETS spectra (for example, location of the P=O and P-O-(H) stretch modes) with the results of these calculations, and with the effectiveness of the molecules in inhibiting hydration of aluminum oxide in the presence of moisture. An analysis of our results for these two modes is given below.

The locations and relative strengths of the P=O and P-O-(H) IETS stretch frequencies among PA, HMP, and NTMP listed in Tables I, II, and III are agin listed here for convenience.

IETS:	P=O	P-O-(H)
PA	1170 (b)	1085 (m)
HMP	1210 (vs)	1055 (vs)
NTMP	1200 (b)	1040 (vs)

The frequencies for NTMP adsorbed on aluminum oxide, and the Al-NTMP complex formed by reacting Al $(NO_3)_3$ with NTMP were as follows:

FT-IR:	P=O	P-O-(H)
Dried	1188-970	1188-970
oxide adsorbed	1256	1052
Al-complex	1160	----

The IETS spectra showed much stronger features for these two modes than did the PA and NTMP. The locations of the IETS P=O modes at 1170, 1210 and 1200 cm^{-1} when compared with the (maximum) value from the dried NTMP spectrum suggests that the frequency for the P=O mode was increased by adsorption on the oxide.

Any shift which might have occurred in the P-O-(H) frequency cannot be determined on the same basis since the location of the P-O-(H) frequency for the dried NTMP is not well determined by the FT-IR data. Some progress can be made in the analysis of the P-O-(H) modes, however, by comparison with solution data from the literature. Veken and Herman[1] found the P=O stretch frequency near 1140 cm^{-1} for dilute solutions of H_3PO_3 in water (i.e., near the 1170 cm^{-1} value for IETS PA). The $P-(OH)_2$ antisymmetric and symmetric stretch frequencies were near 1010 and 950 cm^{-1}, respectively, and the corresponding IR frequencies were near 1005 and 960 cm^{-1}, in good agreement. These data suggested that both the P=O and P-O-(H) observed stretch frequencies were increased by adsorption--as were the P=O modes. From these upward shifts we conclude that the phosphonate groups were significantly perturbed by adsorption on the oxide, and that these groups in PA, HMP and NTMP were active in the formation of bonds to the surface.

E. Summary

Observed upward shifts in the P=O and P-O-(H) stretch frequencies observed in the IETS spectra as compared to values from FT-IR, IR and Raman data taken on dried, complexed and solution samples strongly suggests that PA, HMP and NTMP bond to aluminum oxide through the phosphonate group.

For further analysis it would be useful to have frequency values for PA, HMP and NTMP in solution.

The absence of IETS intensities for tunnel junctions doped with MPA indicates that it does not bond nearly as strongly as do PA, HMP and NTMP. On this basis it would be judged as a poor inhibitor candidate. This conjecture was found to be in agreement with results from wedge tests.

III. Calculation of IETS Intensities

A. Model Considerations

The fact that IETS can provide both IR and Raman-like modes for monolayer coverages of molecules adsorbed on aluminum oxide makes it obvious that it is an ideal tool for studying bonding and orientation of molecular species to the oxide. Interpretation of IETS spectra can occur at two levels:

1) Use of measured vibrational frequencies and their shifts from values obtained independently (for example, optically) to extract information on the adsorbed species.

2) Comparison of measured and calculated relative peak intensities in an IETS spectrum to obtain information on the orientation and structure of the absorbed species. Regarding Item 1, locations of mode frequencies can be very informative and are often quite sufficient for intended purposes. The use of relative mode intensities is far from simple, however. Sometimes the "orientational selection rule" for IETS is used in a rather qualitative fashion. According to this rule, modes having atomic vibrations which move perpendicular to the oxide surface are much stronger than modes with atomic motions parallel to the surface. To use IETS intensities in a quantitative fashion requires extensive modeling and computation. The extraction of useful information depends on several factors including:

1) The degree to which the model correctly approximates the interaction between the tunneling electron and the molecule, and

2) the values assigned for model parameters including those parameters associated with the molecule of interest.

As part of this work, we have developed an improved model for calculating IETS intensities. These intensities can be calculated as a function of the orientation and structure of the adsorbate. The basis of our model is the so called partial-charge model of Kirtley, Scalapino, and Hansma[4] hereafter called the KSH model. It utilizes a transfer Hamiltonian formalism. We chose this model because it was the most tractable model existing. It is called the partial-charge model since the electron molecule interaction is approximated by a Coulombic interaction between the electron and the partial charges on each atomic site of the molecule. It has been used before by Kirtley, Scalapino, and Hansma to calculate the ratio of peak intensities for the OH ion in both the parallel and perpendicular orientations to demonstrate the orientation effects mentioned above. The primary difficulties associated with this model are twofold:

1) To date there has been no reliable means to correctly assign the atomic partial charges to the atoms, the values of which we have found can greatly influence the peak intensity ratios which are calculated.

2) It is known from other calculations that the pseudodipolar potential seen by the tunneling electron is not always oriented as would be expected from charges moving along the directions of atomic motion. This effect is especially pronounced for modes with significant hydrogen motion.

To solve these two problems, we have developed what we term the floating valence model. The floating valence model solves the two primary problems associated with the KSH theory in the following ways:

1. It provides a reliable means to assign partial charges to the atomic sites. The charges are determined by fitting the electrostatic molecular potential associated with each mode. Our method for determining the partial charges is based on a technique first used by Momany[5], who calculated potential derived (PD) charges in the following manner:

a. He calculated an ab initio molecular electrostatic potential for the molecule using an atomic orbital basis set.

b. He then determined the effective located at each atomic site which would give a classical electrostatic potential equal to that calculated by ab initio process.

The sensitivity of our tunneling calculations clearly shows that these PD charges, which differ significantly from those obtained from population analysis and semi-imperical methods, are highly accurate.

2. By modifying the fitting procedure, we have also solved the second major problem associated with the partial charge model. We divide the charge associated with each atomic site into two portions, the nuclear part and the valence portion. In fitting the molecular electrostatic potential for each vibrational mode, the nuclear charge is forced to follow the motion of the atom. The valence portion, however, is allowed to "float". Its direction and magnitude are determined by the requirement that the total result of the classical potential must match that of the molecular electrostatic potential calculated from the atomic orbital basis, hence the term "floating valence model".

In Sections B through G which follows, we outline some of the essential features of the partial charged model and the application of this model to thiourea. In order to test the internal consistency of our results, calculations were made on both thiourea and urea. A comparison of the calculated and experimental intensities for thiourea has been completed and is now being evaluated. It will become obvious to the reader that the development of the model and the ensuing

calculations are extensive, and in the interest of conciseness many of the details have been omitted in this report. The material in Section D is most relevant for understanding the calculations presented in Section IV regarding the calculation of atomic charges in PA, MPA, and HMP.

B. Partial Charge Model

The KSH[4] model provides a reasonable basis for describing the mechanism for the tunneling interaction, yet is still tractable enough for calculations on a complex molecule. It treats the interaction potential in the barrier (oxide layer) as the sum of the Coulombic potentials present between the tunneling electron and the partial charges located on each atom of the adsorbed molecule. In their theory, the z-axis is considered to be perpendicular to the metal surfaces with z=0 located at the lead electrode; the oxide fills the space $0<z<s$. The n^{th} atom of the dopant molecule is located at $\vec{R}_n = b_n\hat{x} + c_n\hat{y} + a_n\hat{z}$ and the tunneling electron is located at $\vec{r}$. The initial and final states for the electron are eigenfunctions of the zeroth-order Hamiltonian $\hat{H} = -(\frac{h^2}{2m})\vec{\nabla}^2 + U(\vec{r})$, and they are localized in the volumes $z>s$ and $z<0$, respectively. Outside the barrier, the wavefunctions are propagating waves in the $\hat{x}$ and $\hat{y}$ directions and standing plane waves in the $\hat{z}$ direction. Inside the oxide layer, they oscillate in the $\hat{x}$ and $\hat{y}$ directions and decay exponentially in the $\hat{z}$ direction. The WKB approxiations to the initial and final wavefunctions inside the barrier are given by:

$$\phi_i = \frac{1}{\sqrt{2}L^{3/2}} \frac{\sqrt{k_z}}{\sqrt{\kappa_z}} e^{-\kappa_z(s-z)} e^{i(k_x x + k_y y)}$$

$$\phi_f = \frac{1}{\sqrt{2}L^{3/2}} \frac{\sqrt{k_z'}}{\sqrt{\kappa_z}} e^{-\kappa_z' z} e^{i(k_x' x + k_y' y)}$$

where

$$\kappa_z = [\frac{2m}{}(\phi - E_z)]^{1/2}$$

$$E_z = E - (\frac{h^2}{2m})(k_x^2 + k_y^2)$$

and similar equations hold for the primed states. E is the electron energy relative to the bottom of the conduction band, and L is a normalization length which cancels out later in the calculations. If we assume that the atomic potential can be represented by static charges attached to the vibrating atoms and include screening and image effects, then we arrive at an interaction potential of the following form:

$$V^k(\vec{r}) = \sum_{p=-\infty}^{\infty} \sum_n \frac{-e}{\varepsilon} \vec{\mu}_n^{\,k} \cdot \vec{\nabla}_n \left(\frac{1}{\vec{r}-\vec{R}_n^{\,o}-2ps\hat{z}} - \frac{1}{\vec{r}-\vec{R}_n^{\,o}-(2ps-2a_n)\hat{z}} \right)$$

where

ε = dielectric constant for $Al_2O_3 \approx 3$

n = atomic index

k = vibrational mode index

$\vec{\mu}_n^{\,k} = z_n^{\,k} \delta\vec{R}_n^{\,k}$

$z_n^{\,k}$ = partial charge of the n^{th} atom in the k^{th} mode

$\delta\vec{R}_n^{\,k}$ = displacement of the n^{th} atom in the k^{th} mode

$\vec{R}_n^{\,o}$ = equilibrium position of the n^{th} atom.

Fermi's "golden rule" gives the transition rate across the barrier ($w_{if}^{\,k}$) as:

$$w_{if}^{\,k} = \left(\frac{2\pi}{\hbar}\right) |M_{if}^{\,k}|^2 \delta(\varepsilon_i - \varepsilon_f - \hbar\omega_k)$$

where

ε_i = initial electron energy

ε_f = final electron energy

$M_{if}^{\,k} = \int_0^l \phi_f^* V^k(\vec{r}) \phi_i d^3x$.

To find the IETS current, we multiply the transition rates by 2e (2 for the spin sum) and sum over all initial and final wave vector states. In the low temperature limit, the wave vector sums become integrals which are expressed in spherical coordinates. After performing all possible analytical integrations and differentiating twice with respect to eV we obtain:

$$\frac{d^2 i^k}{d(eV)^2} = \frac{8e^3m^3N}{\varepsilon^2\hbar^7\pi^3} \sqrt{\varepsilon_F}\sqrt{\varepsilon_F - eV} \sum_{n,m,\ell,\ell'} (\mu_n^{\,k\ell})(\mu_m^{\,k\ell'}) A_{n,m,\ell,\ell'}^{\,k} \delta(\hbar\omega - eV) \qquad (3.1)$$

where

$$A_{n,m,\ell,\ell'}^{\,k} = \int_0^{2\pi} d\phi_2 \int_0^1 d(\cos\theta) \int_0^1 d(\cos\theta') \langle \alpha_{\ell\ell'} \rangle_{nm} \alpha_\perp c_n^{\,k\ell} \alpha_\perp c_m^{\,k\ell'} \qquad (3.2)$$

$$\alpha_\perp c_n^{k\ell} = \zeta_z e^{-\kappa_z s}\frac{\alpha_\perp}{\alpha_\perp}\{\frac{(e^{\alpha_\perp z_n} \pm e^{-\alpha_\perp z_n})}{2s\alpha_\perp}(\frac{e^{(\alpha_z-\alpha_\perp)s}-1}{\alpha_\perp-\alpha_z}+\frac{e^{(\alpha_z+\alpha_\perp)s}-1}{\alpha_\perp+\alpha_z})$$
$$+\frac{1}{\alpha_\perp-\alpha_z}[e^{(\alpha_z-\alpha_\perp)s}(e^{\alpha_\perp z_n}\pm e^{-\alpha_\perp z_n})-(e^{\alpha_z z_n}\pm e^{-\alpha_\perp z_n})]$$
$$\pm\frac{1}{\alpha_\perp+\alpha_z}(e^{\alpha_z z_n}-e^{-\alpha_\perp z_n})\} \qquad (3.3)$$

$\mu_n^{k\ell} = Z_n^k \delta_n^{k\ell}$

$\delta_n^{k\ell}$ is the displacement of the n^{th} atom in the k^{th} mode in the ℓ^{th} Cartesian direction

[Note that the upper signs go with ℓ=3 (z direction), lower signs go with ℓ=1,2 (x,y directions), and the $\alpha_\perp/\alpha_\perp$ factor in Eq. (3.3) is not an error. It corrects a typographical error in the paper by Kirtley, et al.[6]]

$\alpha_x = k_x - k_x'$

$\alpha_y = k_y - k_y'$

$\zeta_z = (k_z k_z'/\kappa_z\kappa_z')^{1/2}$

$\alpha_\perp = (\alpha_x^2+\alpha_y^2)^{1/2}$

$\alpha_z = \kappa_z - \kappa_z'$

$$\langle\alpha_{11}\rangle_{nm} = 2\pi[\frac{b_{nm}^2}{\rho_{nm}^2}J_o(\alpha_\perp\rho_{nm}) - (\frac{b_{nm}^2-c_{nm}^2}{\rho_{nm}^3\alpha_\perp})J_1(\alpha_\perp\rho_{nm})] \qquad (3.4)$$

$$\langle\alpha_{12}\rangle_{nm} = \langle\alpha_{21}\rangle_{nm} = 2\pi\frac{b_{nm}c_{nm}}{\rho_{nm}^2}[J_o(\alpha_\perp\rho_{nm}) - \frac{2}{\alpha_\perp\rho_{nm}}J_1(\alpha_\perp\rho_{nm})]$$

$$\langle\alpha_{22}\rangle_{nm} = 2\pi[\frac{c_{nm}^2}{\rho_{nm}^2}J_o(\alpha_\perp\rho_{nm}) + (\frac{b_{nm}^2-c_{nm}^2}{\rho_{nm}^3\alpha_\perp})J_1(\alpha_\perp\rho_{nm})]$$

$\langle\alpha_{13}\rangle_{nm} = \langle\alpha_{23}\rangle_{nm} = \langle\alpha_{31}\rangle_{nm} = \langle\alpha_{32}\rangle_{nm} = 0$

$\langle\alpha_{33}\rangle_{nm} = 2\pi J_o(\alpha_\perp\rho_{nm})$

$b_{nm} = b_n - b_m$

$c_{nm} = c_n - c_m$

$\rho_{nm} = (b_{nm}^2 + c_{nm}^2)^{1/2}$.

The change in conductance due to the k^{th} vibrational mode is found by integrating Eq. (1) over eV:

$$\Delta(\frac{d_j}{d(eV)})^k = \frac{8e^3m^3N}{\epsilon^2h^7\pi^3}\sqrt{\varepsilon_F}\sqrt{\varepsilon_F'-eV}\sum_{n,m,\ell,\ell'}(\mu_n^{k\ell})(\mu_m^{k\ell'})A_{n,m,\ell,\ell'}^k \; . \qquad (3.5)$$

In reality, the theoretical delta function of Eq. (3.1) is experimentally broadened into a Gaussian so we have the alternate form:

$$\Delta\left(\frac{d^k j}{d(eV)}\right) = \frac{8e^3m^3N}{\varepsilon^2h^7\pi^3}\frac{1}{\sqrt{2\pi}\sigma_k}\int\sqrt{\varepsilon_F}\sqrt{\varepsilon_F'-eV}\sum_{n,m,\ell,\ell'}(\mu_n^{k\ell})(\mu_m^{k\ell'})A_{n,m,\ell,\ell'}^{k}$$

$$\times \exp\left[-\frac{1}{2}\left(\frac{E_k-eV}{\sigma_k}\right)^2\right] d(eV) \quad . \qquad (3.6)$$

Finally, we use Eq. (3.6) to calculate the theoretical ratios between the intensities of the j^{th} and k^{th} modes, and we compare these ratios to the I_{jk} values which were experimentally determined.

A careful study of Eqs. (3.1)-(3.6) shows that four pieces of information are required in order to calculate theoretical intensity ratios, namely:

1. The structure of the adsorbed molecule. This yields the relative atomic coordinates (b_n, c_n, a_n) for each atom in the molecule.
2. The peak widths, centers, and amplitudes for each of the Gaussian functions used to approximate the experimental tunneling peaks.
3. The atomic displacements for each atom during each vibrational mode. This gives us the $\delta_n^{k\ell}$ of the theory.
4. The partial charges, z_n, for each of the atoms in the adsorbate.

Items 1, 2, and 3 will be discussed in more detail in Section C. The calculation of partial charges will be described in Section D.

Kirtley, Scalapino, and Hansma have used the KSH theory to calculate tunneling intensities for a hydroxyl ion adsorbed on an aluminum oxide surface, and Kirtley and Hall[6] have successfully calculated tunneling intensities for the methyl radical of the methyl-sulfonate ion chemisorbed on alumina. However, both of these applications involve small, highly symmetric molecules (or radicals), with only two atom types. An interesting question is whether or not the KSH theory can accurately explain the tunneling spectra of the larger, more complex molecules of general interest in these inhibitor studies. In order to answer this question, we studied thiourea,

chemical formula $SC(NH_2)_2$, adsorbed on aluminum. Thiourea has been shown to be a planar molecule with C_{2v} symmetry and five "atom types," so it is sufficiently complex to experimentally test the validity of the KSH theory. In addition, we believed that development of this model using thiourea would provide valuable insights into the validity of various calculational procedures which would not be possible by first using a molecule as complex (structure, atom type, and symmetry) as PA or MPA. Our approach has been justified as this report indicates.

C. Experimental Results for Thiourea and Urea

As mentioned previously, we must know the structure of a molecule if we are to calculate relative tunneling intensities. Several studies indicate that the thiourea molecule is either planar or very nearly planar. We have assumed a planar geometry.

Many of the calculations which we performed for thiourea in this study were repeated for urea to check internal consistency. Urea has an oxygen atom substituted for the sulfur atom in thiourea which results in a significantly shorter carbon-chalcogen bond length in urea.

The tunneling spectrum for thiourea corrected for the elastic contribution is shown in Fig. 4a and 4b. It has been enlarged and digitized and the resulting experimental peak structure fitted with a superposition of Gaussians. The program varied the amplitude, halfwidth, and center of each Gaussian, denoted by A_i, ω_i, and M_i respectively, until a "best fit" was obtained with the data. The results of this fit, the final A_i, ω_i, and M_i values, are used to calculate the experimental intensity ratio between any two peaks (I_{jk}) via the relationship $I_{jk}=A_j\omega_j/A_k\omega_k$. We used relative rather than absolute intensities throughout this study because the former allowed us to use uncalibrated experimental spectra.

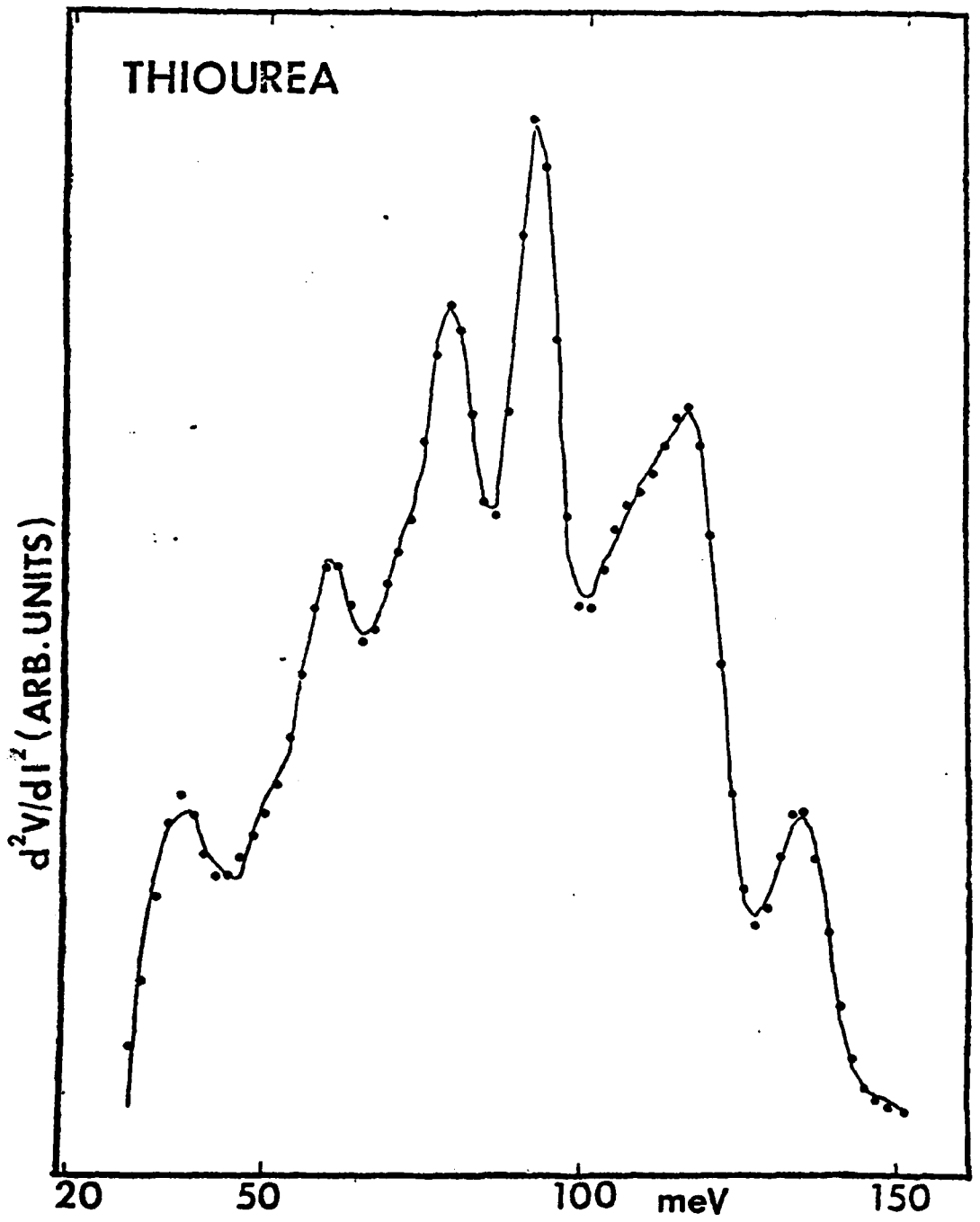

Fig. 4(a). Background-corrected tunneling spectrum of thiourea from 20 to 150 meV

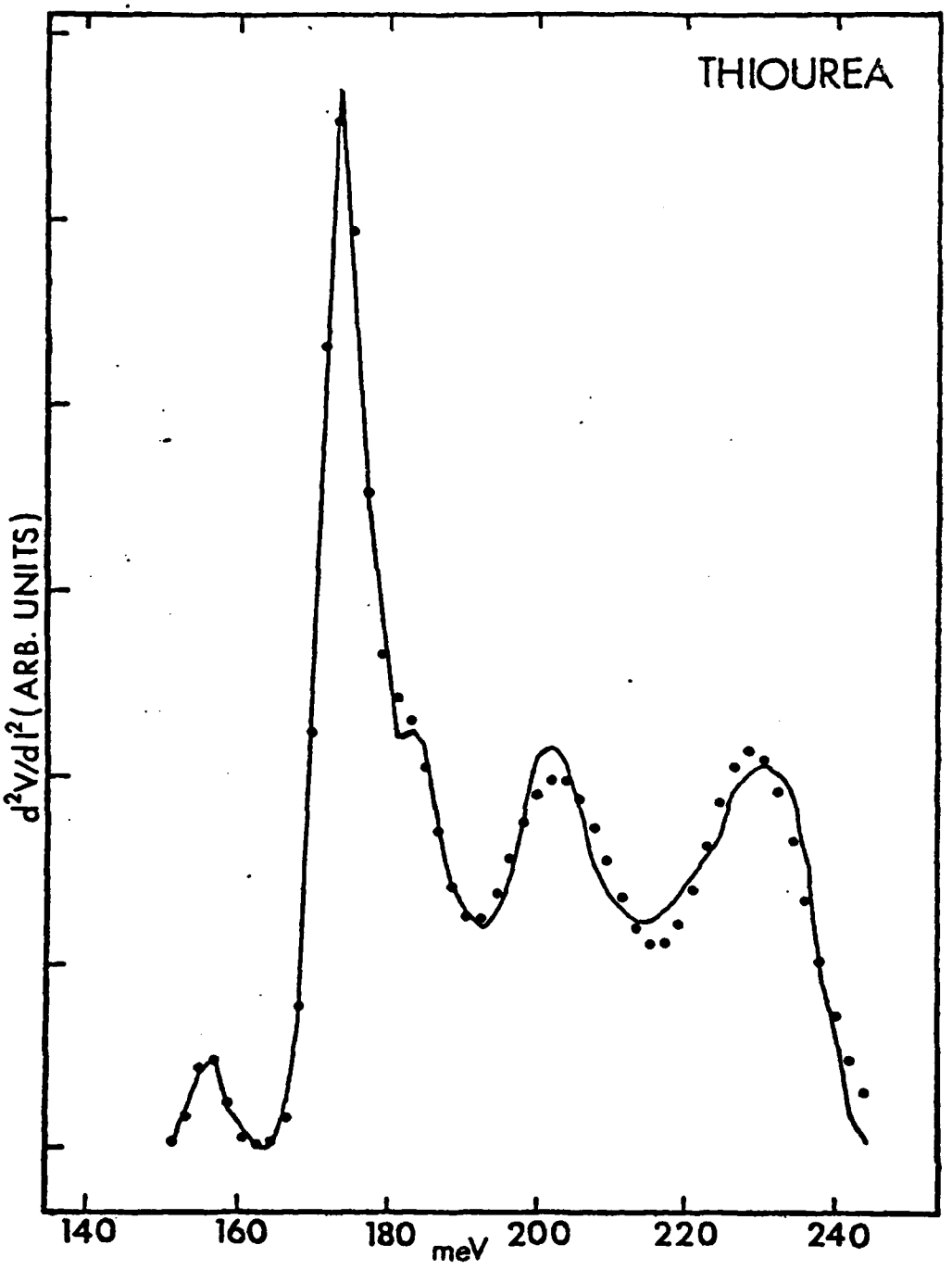

Fig. 4(b). Background-corrected tunneling spectrum of thiourea from 150 to 240 meV.

Table IV. Tunneling peak energies and vibrational mode assignments for thiourea from 30 to 250 meV. The following abbreviations have been used: IP for in plane modes; OP for out of plane modes. Stewart[1] did not provide uncertainties with his frequencies.

Energy (meV)	Frequency Approximate (cm^{-1})	Frequency Reference (cm^{-1})	Assignment
36.2±1.2	292±10		Aluminum phonon
48.1±5.4	388±40	415±4[2]	SCN_2 rock[2] (IP)
60.8±2.2	490±17	468±5[2]	CN_2 deformation[2] (IP)
		505[1]	NH_2 torsion[1] (OP)
		483[3]	NH_2 torsion[3] (OP)
69.5±0.7	561±6	577[1]	NH_2 wag[1] (OP)
78.8±0.3	635±2	629[1]	Skeletal vibration[1] (OP)
92.1±0.2	743±2	732±7[2]	NH_2 rock[2] (IP)
		769[1]	NH_2 wag[1] (OP)
105.8±2.0	853±16		Combination mode SCN_2 Rock + CN_2 deformation
118.0±1.2	952±10		Oxide Phonon
134.5±3.0	1085±2	1088±11[2]	NH_2 deformation[2] (IP)
155.4±0.7	1253±6		2xSkeletal vibration
173.1±0.2	1396±2	1415±4[2]	CS stretch[2] (IP)
181.2±1.0	1462±8	1470±15[2]	NH_2 deformation[2] (IP)
202.3±0.6	1632±5	1620±16[2]	CN_2 asym stretch[2] (IP)
		1628±16[2]	CN_2 sym stretch[2] (IP)
228.5±0.5	1843±4		2xOxide phonon

[1]J.E. Stewart, J. Chem. Phys. 26, 248 (1956).

[2]G.B. Aitken, J.L. Duncan, and G.P. McQuillan, J. Chem. Soc. (A), 2695 (1971).

[3]Stewart's mode assignment, frequency corrected by Aitken, et al.[1]

The fitted peak structure agrees well with the background corrected experimental data as shown in Figs. 4(a) and 4(b). We referenced several infrared and Raman peak assignments and found that the peak assignments of Aitken, Duncan, and McQuillan[7] for the in plane modes gave the best agreement with our tunneling results. Similarly, we have generally used the assignments of Stewart[7] for the out of plane modes. However, Aitken, et al.[7] have demonstrated conclusively that Stewart incorrectly assigned the mode at 58 meV. Consequently, we have used Aitken's value for the lowest out of plane frequency. Table IV shows IETS peak centers and mode assignments which have been made on the basis of several studies in the literature. Table IV also illustrates the resolution problems which occur in IETS. The peaks at 202.3, 134.5, and 92.1 meV are doublets, and the peak at 60.8 meV is a triplet. We could not resolve these peaks, and they caused some problems in the theoretical analysis.

We eliminated from further consideration those peaks which resulted from aluminum, aluminum-oxide phonons, combination modes and overtones. We chose the peak at 181.2 meV as the normalization peak for relative intensities because it turned out to be very stable with regard to orientation in the theoretical calculations.

For small displacments, chemical bonds behave like Hooke's Law springs. Consequently, we can treat molecular vibrations by assuming that a molecule is approximated by a system of point masses interconnected through a series of springs. The problem is formulated most elegantly in mass-weighted Cartesian coordinates

We were not fortunate enough to find Cartesian displacements for the vibrational modes of thiourea. Consequently, we searched the literature for force constants which could be used to generate Cartesian displacements. We found several sets of force constants for the planar modes of thiourea which gave frequencies in reasonable agreement with experiment, but only one plausible set for the out of plane modes. In order to generate vibrational displacements, we first had to generate the B matrix for the internal coordinates used by each

author. This was done using Quantum Chemistry Program Exchange (QCPE) #342[9]. Next, we used QCPE #342 to solve for the eigenvalues λ_i which determined the vibrational frequencies ν_i. We found that the force constants of Bleckmann, Schader, and Meier[10] best fit to our observed in plane frequencies. The force constants were iterated slightly to reduce the differences between calculated and observed frequencies. Bleckmann's out of plane force constants did not agree well with our observed frequencies. They changed significantly during the iteration process, and this caused difficulties in the resultant Cartesian displacements. It is very important to emphasize the effect of iteration on the vibrational displacements. Originally, the second highest frequency mode had a calculated frequency of 534 cm^{-1}. After iteration the mode was shifted upward to 632 cm^{-1}, but the mode pattern was essentially unchanged. It turned out that the theoretical intensity for the mode at 635 cm^{-1} (78.8 meV) was the furthest from experimental values. This difference may be entirely due to the initial discrepancies between the observed out of plane frequencies and calculated values.

These observations clearly point out the need for an accurate and complete vibrational mode analysis for any molecule for which tunneling intensity calculations are to be made. For this reason we have chosen to emphasize the use of the partial charge determinations, as presented in Section D, as being perhaps the most constructive application of these calculations. It should be emphasized at this point, however, that the completion of this tunneling intensity calculation has made possible a very critical assessment of the internal steps. As a consequence, we are now able to calculate atomic charges associated with each atom in a molecule using the best method available, and we know the values obtained are reliable and accurate.

D. Partial Charge Determinations

1. Calculation of Molecular Electrostatic Potential

The partial charges for thiourea were calculated using a technique developed by Momany[5] for formamide, methanol, and formic acid. Momany calculated an ab initio molecular electrostatic potential using atomic orbital basis sets. Then he determined the effective partial charge located at each atom site by requiring that their resultant classical Coulomb potential be equal to the potential values obtained by the ab inito process. These potential derived (PD) charges which he obtained differed significantly from those obtained from population analysis and semi-empirical methods. Our studies have shown that relative peak intensities in IETS depend strongly on the partial charges used in the computations, and as a consequence we can state that the PD charges are more accurate than those obtained by other methods. Since these charges are of interest in these inhibitor studies we outline how the molecular electrostatic potentials are obtained, and how the PD charges are thereby obtained.

The ab initio electrostatic potential was calculated using self-consistent Hartree-Fock theory. The basic equation for this theory is

$$\hat{F}\Psi_i = \varepsilon_i \Psi_i \qquad (3.7)$$

where

Ψ_i is the i^{th} molecular orbital

ε_i is the i^{th} energy eigenvalue

$\hat{F}$ is the Fock operator (the effective one-electron operator) defined by

$$\hat{F}(p) = -\frac{1}{2}\nabla_2^2 - \sum_a \frac{Z_a}{r_{ap}} + \sum_j (2\hat{J}_j - \hat{K}_j) \qquad (3.8)$$

where

p is the electron index

a is the atom index

Z_a is the nuclear charge for the a^{th} atom

r_{ap} is the distance from the a^{th} nucleus to the p^{th} electron

$\hat{J}_j$ and $\hat{K}_j$ are the Coulomb and exchange operators which will be defined below

$$\hat{J}_j \Psi_i(p) = \int \Psi_j^*(q)\left(\frac{1}{r_{qp}}\right)\Psi_j(q)d\tau_q \Psi_i(p) \qquad (3.9)$$

$$\hat{K}_j \Psi_i(p) = \int \Psi_j^*(q)\left(\frac{1}{r_{qp}}\right)\Psi_i(q)d\tau_q \Psi_j(p) \qquad (3.10)$$

where

q and p are electron indices

$d\tau$ is a volume element

r_{qp} is the distance between the q^{th} and p^{th} electrons.

In our calculations, we used the linear combination of atomic orbitals (LCAO) approach, which assumes that the molecular orbitals $\Psi_i(\vec{r})$ can be expanded in terms of atom-centered atomic orbitals $\phi_{\mu a}(\vec{r}_a)$ as

$$\Psi_i(\vec{r}) = \sum_a \sum_\mu \phi_{\mu a}(\vec{r}_a) C_i^{\mu a} \qquad (3.11)$$

where

a is the atom index

μ reflects the n, l, and m quantum numbers of the orbital

$\vec{r}$ is a position vector relative to the origin

$\vec{R}_a$ is the position vector of the a^{th} nucleus

$\vec{r}_a = \vec{r} - \vec{R}_a$

and $C_i^{\mu a}$ are expansion coefficients which we wish to determine.

In atomic calculations, Slater type orbitals (STO's) are often used to represent the radial dependence of the atomic orbitals. A normalized STO with principal quantum number n is given by

$$STO_n(r) = N_n r^{n-1} e^{-\zeta r} \qquad (3.12)$$

where

N_n is a normalization constant

and ζ is a parameter which is optimized to give the best fit to the radial dependence of a particular atomic orbital.

Unfortunately, STO's are too unwieldy to use for molecular calculations. One approach to alleviate this difficulty is to use a linear combination of Gaussians to represent the exponential dependence of the STO's. If we let $\phi_\mu(r)$ represent the exponential dependence of an STO, then it can be expanded as follows:

$$\phi_\mu(r) = \sum_{i=1}^{N} d_{i\mu} \exp(-\alpha_i r^2) \qquad (3.13)$$

where

N is the number of Gaussians used in the expansion

$d_{i\mu}$ are contraction coefficients

α_i is the Gaussian exponent.

We used this approach as implemented by Quantum Chemistry Program Exchange (QCPE)#437 (Gaussian 80)[11] to perform our computations. The Gaussian contraction scheme for each orbital is referred to as the basis set. We used several different basis sets in our work, designated by STO-3G, STO 4-31G (4-31G), STO 6-31G (6-31G), STO 4-31G** (4-31G**), and STO 6-31G** (6-31G**).

The Fock operator of Eq. (3.7) depends on the set of Ψ_i's chosen. Gaussian 80 uses optimized atom-centered atomic orbitals [$\phi_{\mu a}(\vec{r}_a)$'s] along with a set of "guessed" $C_i^{\mu a}$'s to calculate an initial $\Psi_i(\vec{r})$'s via Eq. (3.11). (The starting $C_i^{\mu a}$'s are generated from a Hückel or projected Hückel guess). The Fock matrix is determined from the $\Psi_i(\vec{r})$'s via Eqs. (3.8), (3.9) and (3.10) and is used in Eq. (3.7) to solve for new Ψ_i's and ε_i's. This process is repeated until the energy eigenvalues converge. The final wavefunctions yield the optimal set of $C_i^{\mu a}$'s which can be used to calculate the electron density, $\rho(\vec{r})$, from the relationship

$$\rho(\vec{r}) = \sum_{i}^{occ} |\Psi_i(\vec{r})^2| = \sum_{\substack{\mu,a \\ \nu,a'}} \phi_{\mu a}(\vec{r}_a)\phi_{\nu a'}(\vec{r}_{a'}) \sum_{i}^{occ} C_i^{\mu a} C_i^{\nu a'} \qquad (3.14)$$

where $\sum_{i}^{occ}$ indicates that the sum is over occupied orbitals only.

All our calculations used restricted Hartree-Fock theory which assumes that both a spin up and a spin down electron occupy each spatial orbital. Once $\rho(\vec{r})$ has been obtained, the molecular electrostatic potential, $V(\vec{r})$, can be determined since

$$V(\vec{r}) = \sum_{a} \frac{Z_a e}{|\vec{r}-\vec{R}_a|} - e\int \frac{\rho(\vec{r}')}{|\vec{r}-\vec{r}'|} d\vec{r}' \ . \qquad (3.15)$$

In its original form, Gaussian 80 does not calculate $V(\vec{r})$. However, it does perform integrals very similar to those found in Eq. (5.9) when it computes one electron integrals. We modified the STVINT section of Gaussian 80 to do these integral calculations. Once this was done, it was a simple matter to add in the nuclear contributions to the potential [the first term in Eq. (3.15)] to calculate the quantum mechanical electrostatic potential.

We calculated the electrostatic potential for urea and thiourea using the STO-3G, 4-31G, and 4-31G** basis sets. We also used the 6-31G and 6-31G** basis sets for urea only. We made contour plots for both molecules using a variety of basis sets showing equipotential lines, both in the plane of the molecule (yz plane) and perpendicular to the molecular plane (xz plane). In all instances the carbon-chalcogen bond is directed along the positive z-axis. A sample plot for thiourea is shown in Fig. 5.

Similar plots for PA, MPA, and NTMP will be shown in Section IV.

2. Partial Charge Fitting Procedure

Equation (3.15) allows us to determine the molecular electrostatic potential at a point $\vec{r}$. If we are to accurately fit the potential around a molecule with point charges located on atom sites, we must know the quantum mechanical potential for a fairly large, representative set of field points. We calculated the electrostatic potential for urea and thiourea using a rectangular array of equally spaced points. Spatial axes for each molecule were oriented so that the plane of the molecule was the yz plane with the C=O bond or C=S bond directed along the positive z-axis. The origin was chosen at the center of nuclear charge. Since the molecular electrostatic potential is strongly positive near the atom centers, we excluded all field points which were within the van der Waal's radius of any atom. We used a standard statistical package to fit partial charges to the molecular electrostatic potential. Our preliminary results showed that the partial charge determinations were strongly affected by the potential at field points which lay close to the van der Waals radii of the atoms. Since IETS is a long range interaction, we weighted all field points which lay within 1 Å of the van der Waals shells by a factor of 0.25 in the fitting procedure. This weighting is consistent with Momany's[5] method.

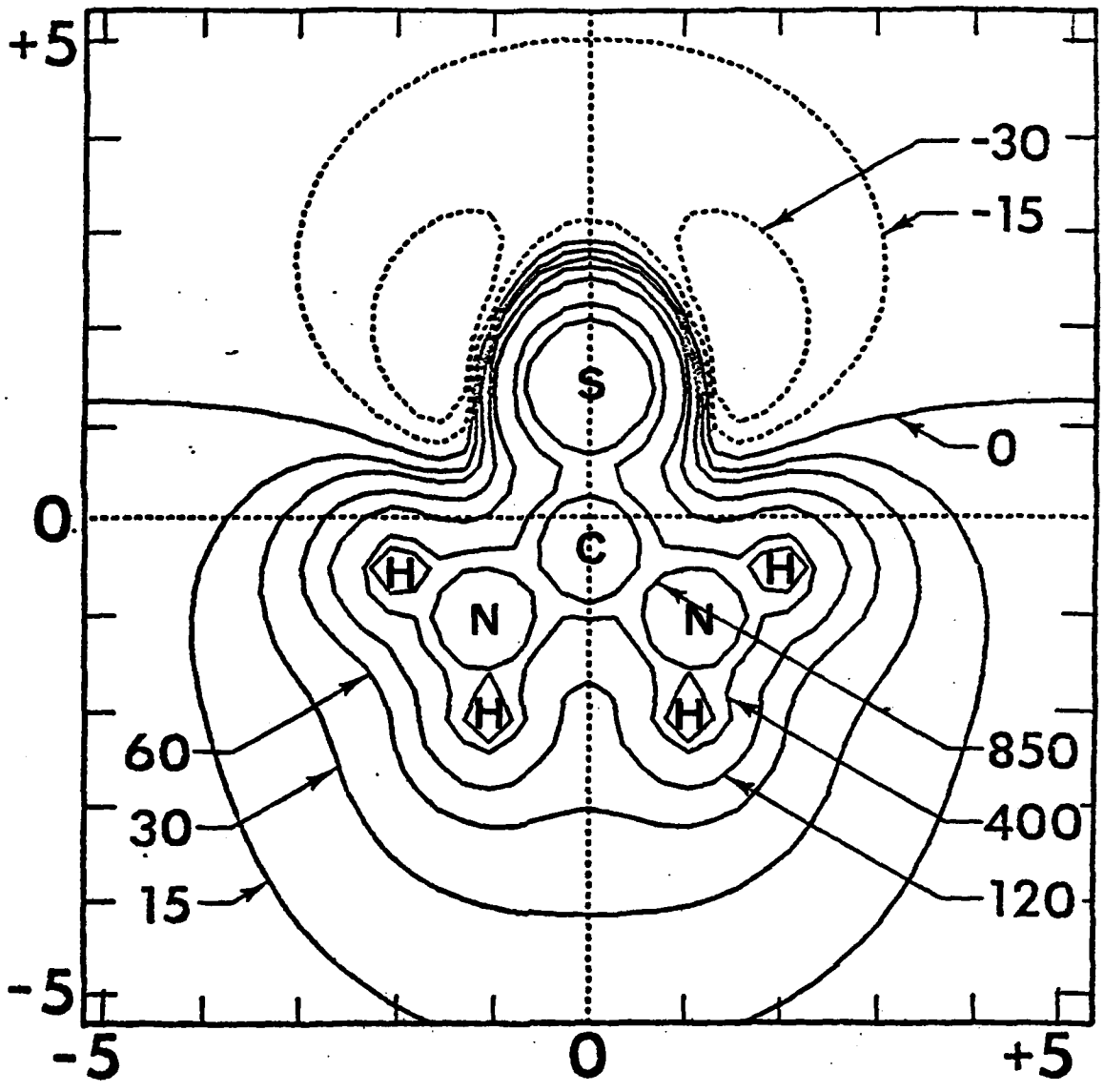

Fig. 5. Electrostatic potential contour plot for thiourea using a 4-31G** basis set. The plot is in the plane of the molecule. Potential values are in Kcal/mole and distances are in angstroms.

E. Static and Dynamic Partial Charges for Urea and Thiourea

Potential derived (PD) charges for urea at equilibrium are given in Table VI for a variety of basis sets. Table VI shows the Mullikan charges for the same basis sets. There are three important conclusions which can be drawn from Tables V and VI. The PD charges calculated from 4-31G and 6-31G basis sets differ by less than 1%. There is also less than a 1% difference between 4-31G** and 6-31G** PD values. Based on these comparisons, we did not use the extremely costly 6-31G basis set, with or without polarization functions, for thiourea calculations. The Mullikan charges calculated from the 4-31G and 6-31G basis sets are in closest agreement to the PD charges. This is an important observation because one would assume that improving a basis set by the addition of polarization functions should yield the most accurate Mullikan charges. There is a large variation in Mullikan charges derived from different basis sets. This strong basis set dependence coupled with our inability to predict which basis would yield the most accurate results make Mullikan charge values unsuitable for accurate IETS intensity calculations.

PD and Mullikan charges for thiourea are presented in Tables VII and VIII It is interesting to compare the PD charges for similar atoms in thiourea and urea. The Mullikan charges for nitrogen and hydrogen atoms in urea vary only slightly from their values in thiourea. On the other hand, the fitted values are significantly different in the two molecules. The sensitivity of the PD charges to the atomic environment led us to use the Potential Derived (PD) computational technique to evaluate the effects of substituting different radicals on phosphoric acid. These calculations are included in Section IV of this report. The difference in the chalcogen and carbon charges in urea and thiourea is striking. It demonstrates the result of lengthening the carbon-chalcogen bond length in thiourea, and the reduced electron affinity of sulfur as compared to oxygen.

Table V. Fitted partial charges for urea.

Atom	STO-3G	4-31G	6-31G	4-31G**	6-31G**
O	-0.537	-0.782	-0.788	-0.693	-0.695
C	0.928	1.279	1.284	1.068	1.073
N_1, N_2	-0.875	-1.193	-1.200	-1.074	-1.085
H_1, H_3	0.338	0.467	0.471	0.440	0.445
H_2, H_4	0.342	0.478	0.481	0.447	0.451

Table VI. Mullikan partial charges for urea.

Atom	STO-3G	4-31G	6-31G	4-31G**	6-31G**
O	-0.346	-0.687	-0.644	-0.687	-0.672
C	0.418	1.022	0.975	0.932	0.936
N_1, N_2	-0.459	-0.926	-0.934	-0.726	-0.766
H_1, H_3	0.199	0.360	0.365	0.284	0.299
H_2, H_4	0.224	0.398	0.404	0.320	0.335

A plot of the quantum mechanical potential for thiourea derived from the 4-31G** basis set minus the Coulomb potential due to partial charges located on atom sites is shown in Fig. 6. The standard of accuracy for a calculation of this type is one Kcal/mole; we have clearly achieved this accuracy with our PD 4-31G** charges. The PD charges give a much better fit to the quantum mechanical potential on the "hydrogen-end" of the molecules than do the Mullikan charges. This result occurs because the Mullikan model allocates shared electrons equally between neighboring atoms with no consideration for the relative electron affinities of different atoms.

The most critical quantities required in order to calculate IETS relative intensities are the $\mu_n^{k\ell}$'s of Eq. (3.6) defined by

$$\mu_n^{k\ell} = Z_n^k \delta_n^{k\ell}$$

where

Z_n^k is the partial charge of the n^{th} atom during the k^{th} vibrational mode

$\delta_n^{k\ell}$ is the displacement of the n^{th} atom during the k^{th} vibrational mode in the ℓ^{th} Cartesian direction.

One of the assumptions which has been made by most researchers in IETS is that Z_n^k is a constant for every vibrational mode and thus $Z_n^k \approx Z_n$, where Z_n is the equilibrium partial charge on atom k. Since we determined that relative peak intensities were very sensitive to the values of the charges, we decided to check the assumption that they remained constant during a molecular vibration. In order to do this, we used the normalized Cartesian displacements discussed earlier to calculate the average position of an atom during a vibrational mode as follows

$$R_n^{k\ell} = R_n^{o\ell} + \delta_n^{k\ell}$$

where

$R_n^{k\ell}$ is the average position of atom n in the ℓ^{th} Cartesian direction during the k^{th} vibrational mode,

$R_n^{o\ell}$ is the equilibrium position of atom n in the ℓ^{th} Cartesian direction.

Table VII. Fitted partial charges for thiourea.

Atom	STO-3G	4-31G	4-31G**
S	-0.427	-0.452	-0.400
C	0.509	0.349	0.166
N_1, N_2	-0.619	-0.672	-0.547
H_1, H_3	0.295	0.377	0.349
H_2, H_4	0.283	0.347	0.316

Table VIII. Mullikan charges for thiourea.

Atom	STO-3G	4-31G	4-31G**
S	-0.204	-0.114	-0.519
C	0.186	0.342	0.642
N_1, N_2	-0.426	-0.884	-0.680
H_1, H_3	0.202	0.366	0.289
H_2, H_4	0.233	0.404	0.330

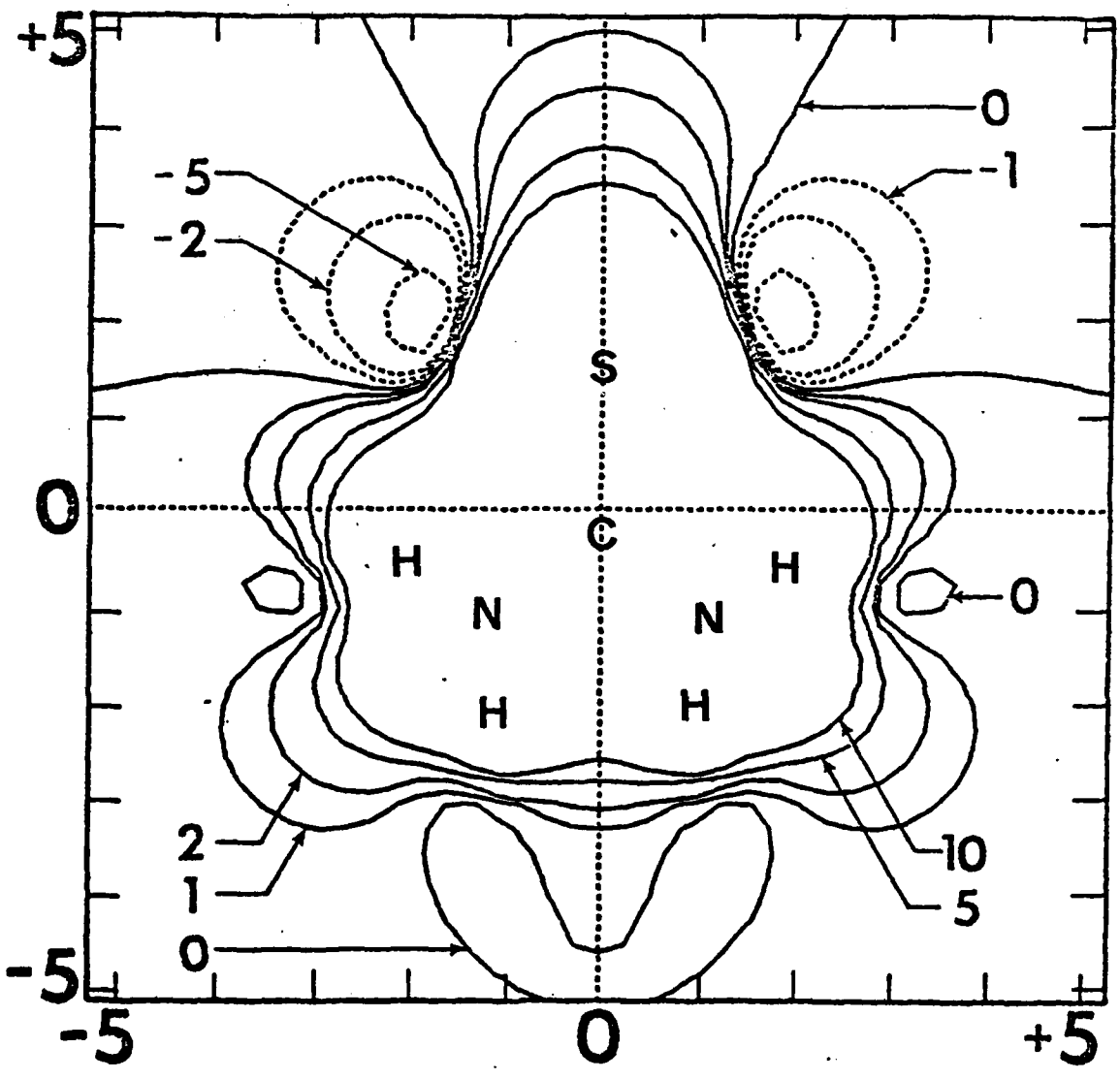

Fig. 6. Potential difference plot for thiourea at equilibrium in the plane of the molecule. The difference is between the potential calculated with a 4-31G** basis set minus split charge (floating) partial charges on the atom sites.

Once we knew the new atom positions, we recalculated the quantum mechanical electrostatic potentials for urea and thiourea and refitted the atomic partial charges as described in Sec. D.2. There is a significant change in the charges during many of the vibrational modes from their equilibrium values, and these have been incorporated into the floating valence model calculations for thiourea.

F. Comparison of Calculated and Experimental Intensities for Thiourea

The calculations have been completed for the relative peak intensities of thiourea as a function of several parameters and are now in the process of being evaluated. Some of the results from this calculation are shown in Table IX with values for several adjustable parameters indicated. These paramenters include basis set, orientation of the molecule with respect to the oxide layer, distance from the oxide to the "adsorbed" molecule, and whether or not the valence charge was allowed to float. Comments made near the end of Section D point out the uncertainty associated with one of the modes which arose in our attempts to iterate the force constants.

G. Summary

We have examined the KSH[4] model for calculating theoretical peak intensities for IETS spectra. Based on our work, we can state the following conclusions:

1. Relative intensities in IETS studies are very sensitive to the choice of atomic partial charges. Consequently, we used the highly accurate technique developed by Momany[5] to determine these charge values for urea and thiourea.
2. We used Momany's technique to examine the effect of a vibrational mode on the electrostatic potential of molecules. We found that the charges needed to fit the vibrational mode potential differed significantly from equilibrium values. These differences led us to develop the floating valence model which uses a core and an electron charge for each atom.

3. The floating valence model significantly improved the quality of our fit to the quantum mechanical potentials of urea and thiourea at equilibrium. We also found that it allowed us to fit the potential during a molecular vibration. In order to achieve this fit, we let the valence charge displace freely during the vibrational mode in such a manner as to minimize the difference between the quantum mechanical potential and the Coulomb potential resulting from the point charges. We found that the core and valence displacements differed significantly for hydrogen atoms. It explains the difficulty which we have had in IETS in analyzing modes which contain a great deal of hydrogen motion.
4. We found that the floating valence model gave an order of magnitude better agreement between theoretical and experimental peak intensities than the original KSH single atomic charge model. We did not quite obtain the accuracy we desired; however, a major difficulty was that we could not find a satisfactory vibrational mode analysis for the out of plane modes of thiourea. Our study clearly demonstrated that precise vibrational analyses are necessary for accurate IETS intensity calculations.
5. The steps in this calculation have yielded valuable insight into the accuracy of various methods for calculating atomic charges within molecules. The potential derived (PD) charges are much more accurate than those obtained from Mullikan population analysis or from semi-empirical techniques.
6. The potential derived (PD) technique should be useful for calculatiing atomic charge distributions in a wide variety of inhibitor molecules.

Table IX. Relative intensities of the IETS peaks of thiourea calculated with the floating valence model using PD 4-31G** charges and iterated force constants for the out of plane modes. The minimum height of the closest atom of thiourea to the surface is 1.5 Å. All centers and widths are in meV's, all orientation angles are in degrees and all force constants are in mdyn/Å.

Center→	202.3[1]	181.2	173.1	134.5[2]	92.1[3]	78.8	69.5	60.8[4]	48.1
Width→	20.9	11.8	6.7	10.3	8.7	13.6	6.3	12.5	13.9
Exper. Rel. Inten.→	1.59	1.00	1.28	1.50	3.59	5.31	0.56	3.15	1.61
Orientation α,β,γ ↓									
0,0,0	0.85 0.43 ≈1.28	1.00	0.30	0.20 0.53 ≈0.73	0.24 1.04 ≈1.28	0.50	1.08	0.22 0.07 | 0.74 0.45	1.16
0,45,0	1.45 2.61 ≈4.06	1.00	0.47	0.11 0.44 ≈0.55	0.30 1.54 ≈1.84	0.56	1.82	0.22 0.07 | 0.74 0.45	1.20
0,180,0	3.70 3.55 ≈7.25	1.00	2.58	0.48 2.13 ≈2.13	0.38 4.48 ≈5.22	1.48	6.62	0.95 0.26 | 1.71 0.50	0.89
0,90,0	1.38 2.96 ≈4.43	1.00	0.59	0.12 0.63 ≈0.75	0.23 2.20 ≈2.43	0.44	2.99	0.40 0.08 | 0.91 0.43	0.90
0,90,90	2.04 2.39 ≈4.43	1.00	1.46	0.65 0.89 ≈1.54	0.33 24.18 ≈24.51	4.46	31.2	1.23 0.57 | 7.59 5.79	0.46

[1]Individual peaks were assumed to have a width of 12 meV.
[2]Individual peaks were assumed to have a width of 10.3 meV.
[3]Individual peaks were assumed to have a width of 8.7 meV.
[4]Individual peaks were assumed to have a width of 12.5 meV.

IV. Atomic Charge Distributions for PA, MPA, and HMP

A. Structure Determinations

In order to determine the potential derived (PD) atomic charges for the inhibitor molecules, it was necessary to determine their structure by suitable methods. Reliable values could not be found in the literature. Our approach was to start with a reasonable structure (or structures in the case of MPA) with best guess values for bond lengths and angles and to utilize our Gaussian 80 QCPE program to optimize the bond lengths and angles based on a minimum energy technique. One of the two structures assumed for MPA was the eclipsed methyl group, denoted as MPA-E. The other structure, denoted as MPA-S, had a staggered methyl group with respect to the P=O bond. The minimum energies obtained for MPA-E and MPA-S were so close as to preclude a decision on which structure was more stable.

The bond angles and bond lengths for PA, MPA, and HMP were calculated with this technique. The results, listed in Tables X through XIII, are consistant with angles and bond length values for related compounds found in the literature.

B. Molecular Electrostatic Potentials

Molecular electrostatic potentials were obtained for each of the structures mentioned in the same fashion as were done for thiourea and urea described earlier. Plots of equipotential lines through high symmetry planes using a 4-31G** basis set are shown in Figs. 7-10 for PA, MPA-E, MPA-S, and HMP. Two basis sets, STO-3G and 4-31G, were used to investigate the effects of basis set selection.

Inspection of Figs. 7-10 reveals significant changes in the charge distribution surrounding the phosphorous atom. These changes depend on the nature of the attached group. The effect of basis set was also apparent. We are currently evaluating these results with the hope that systematic patterns will emerge which can be related to inhibitor effectiveness or to IETS spectral features.

C. Potential Derived charges

The net PD charges for each of the stuctures were obtained by the fitting process outlined earlier. In Tables XIV and XV the net PD charges, as well as the Mullikan values, are shown when obtained from potentials calculated using STO-3G and 4-31G basis sets,

respectively. The basis set influences both the Mullikan and PD values. However, the charges associated with the net charges on each atom site do not necessarily follow the same trend for the Mullikan and PD methods. Note in Table XV the net charge on the phosphorus atom in the sequence PA : MPA-E : MPA-S : HMP is + 2.29 : +1.96 : + 1.94 : + 1.97 using the Mullikan population technique; whereas, it is + 2.17 : + 1.97 : + 2.03 : + 1.72 for the PD fitted technique. The difference in the trend occurs on going from the eclipsed to the staggered configuration of MPA.

We are also attempting to relate the trends in the PD charges on each atom with inhibitor effectiveness, or with features in the tunneling spectra.

D. Summary

A summary from our work on atomic charge distribution calculations is as follows:

1. Our original plans were to do intensity analyses for PA, MPA, HMP, and NTMP, but our study on thiourea showed us that this was not feasible, since detailed vibrational mode analyses have not been done for these molecules. Fortunately our potential derived charges have an application to these large inhibitor molecules. The sensitivity of the PD method allowed us to evaluate charge trends when different end radicals were substituted onto a molecular framework. We are attempting to correlate these trends with important features in IETS spectra such as the frequencies for bond-stretching motions. We would like to use our technique to provide a guage of inhibitor effectiveness.
2. In order to relate PD charge trends for large inhibitors to inhibitor effectiveness and IETS spectral features more, and larger, molecules would need to be analyzed. The use of semi-empirical methods to optimize molecular structures should allow calculation of charges for molecules as large as 100 atoms.

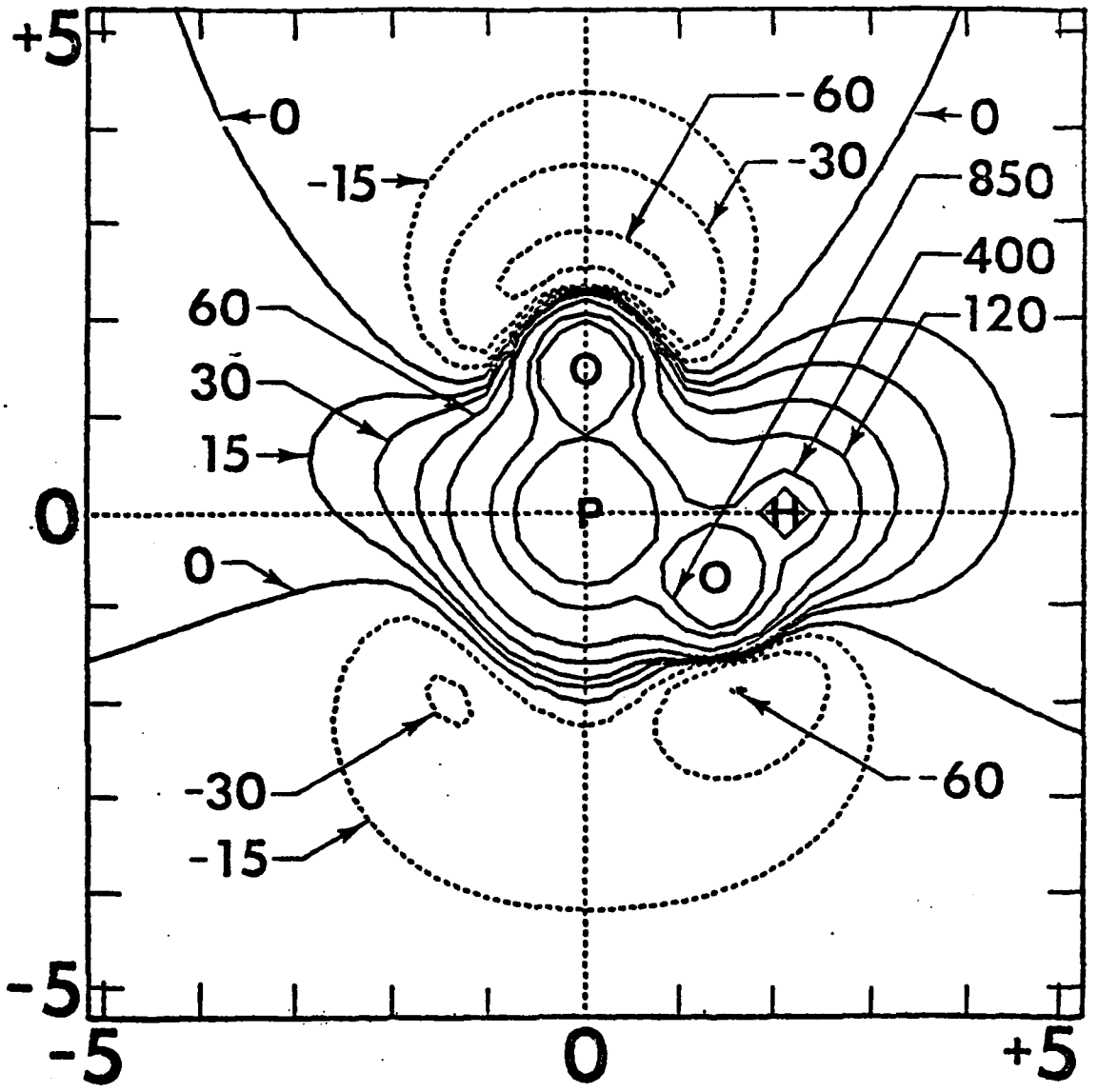

Fig. 7. Electrostatic potential contour plot for PA in the plane of reflection symmetry using a 4-31G basis set. Potential values are in Kcal/mole and distances are in angstroms.

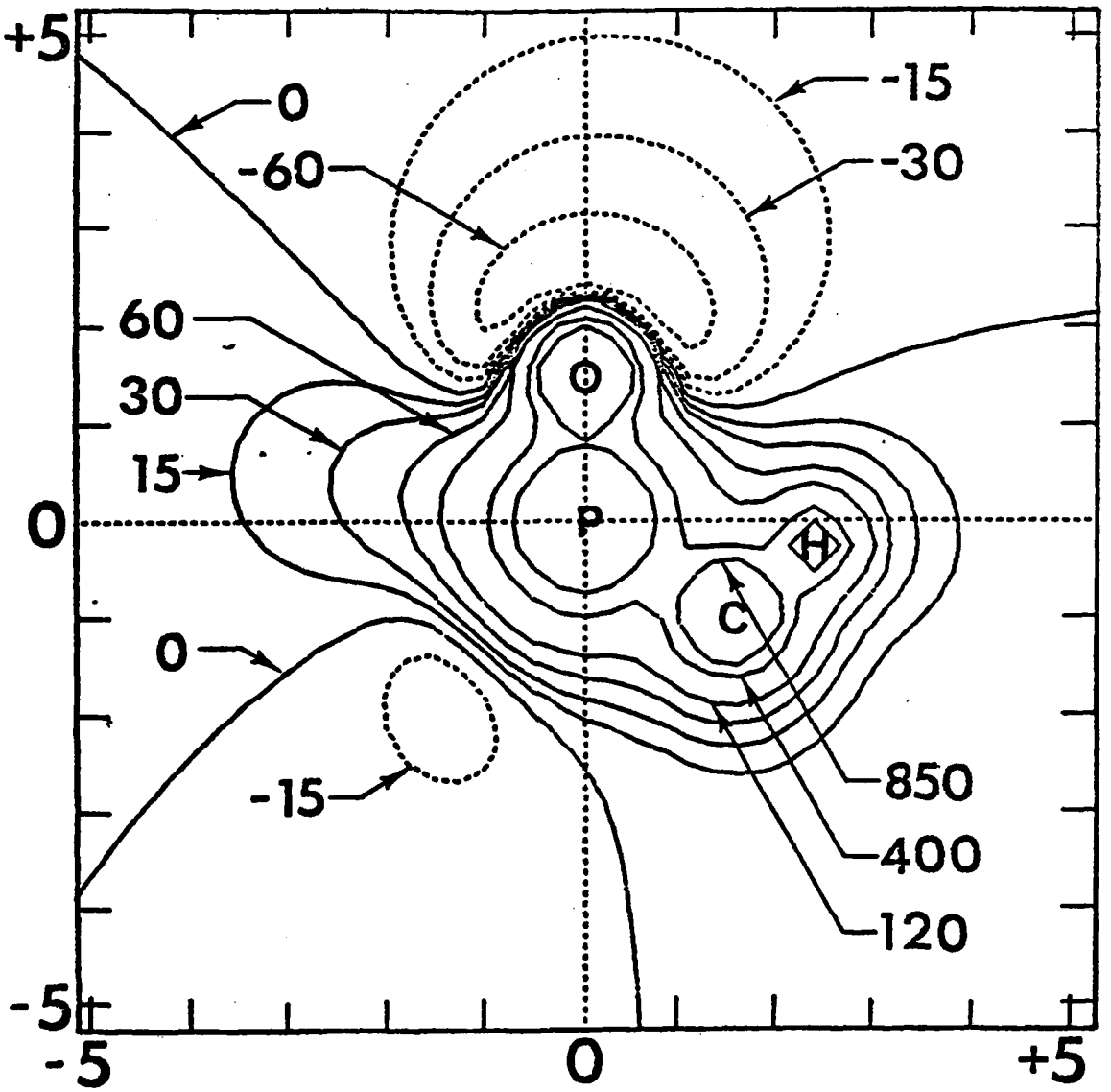

Fig. 8. Electrostatic potential contour plot for MPA-E (eclipsed methyl group with respect to the P=O bond) in the plane of reflection symmetry using a 4-31G basis set. Potential values are in Kcal/mole and distances are in angstroms.

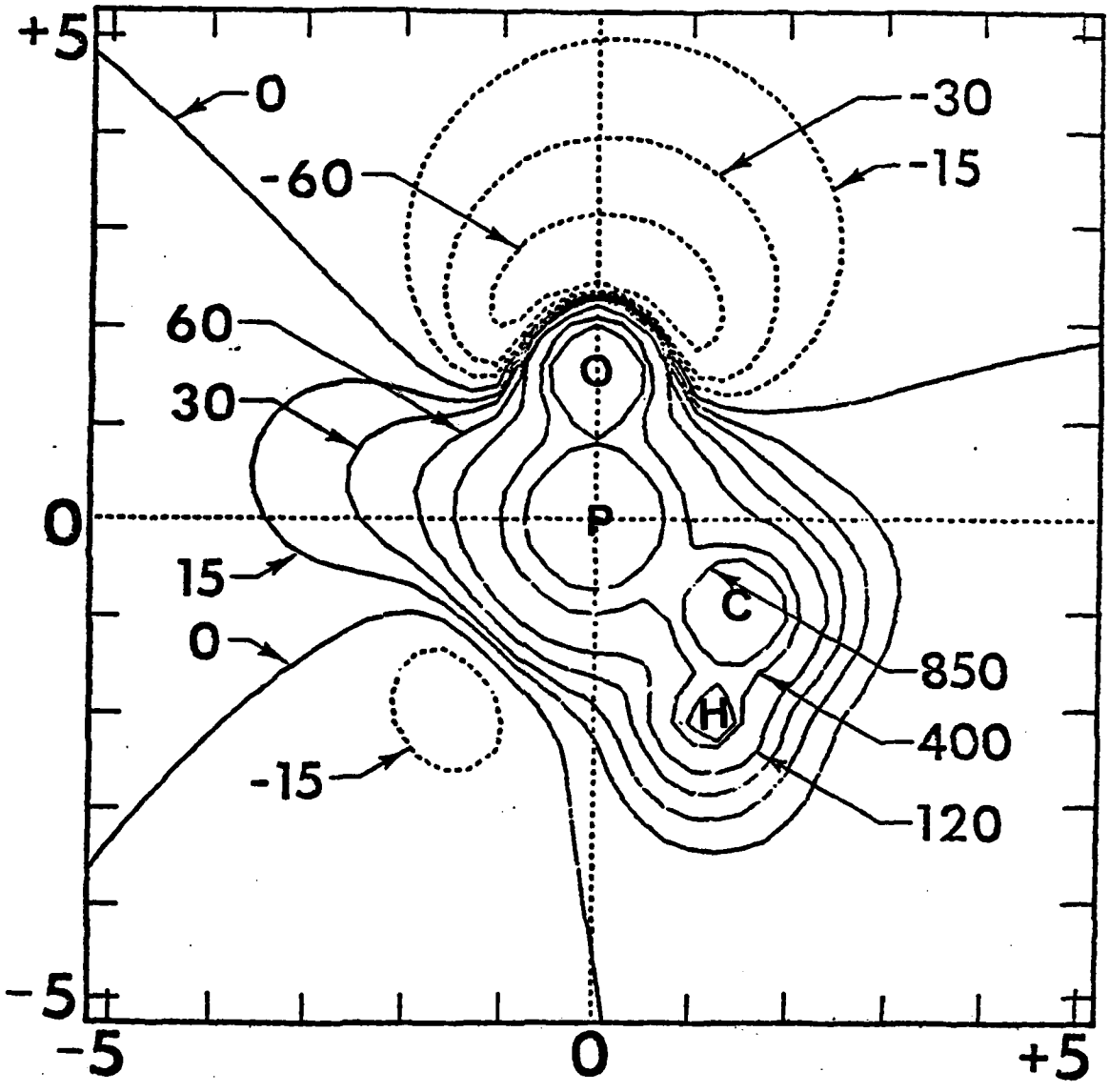

Fig. 9. Electrostatic potential contour plot for MPA-S (staggered methyl group with respect to the P=O bond) in the plane of reflection symmetry using a 4-31G basis set, Potential values are in Kcal/mole and distances are in angstroms.

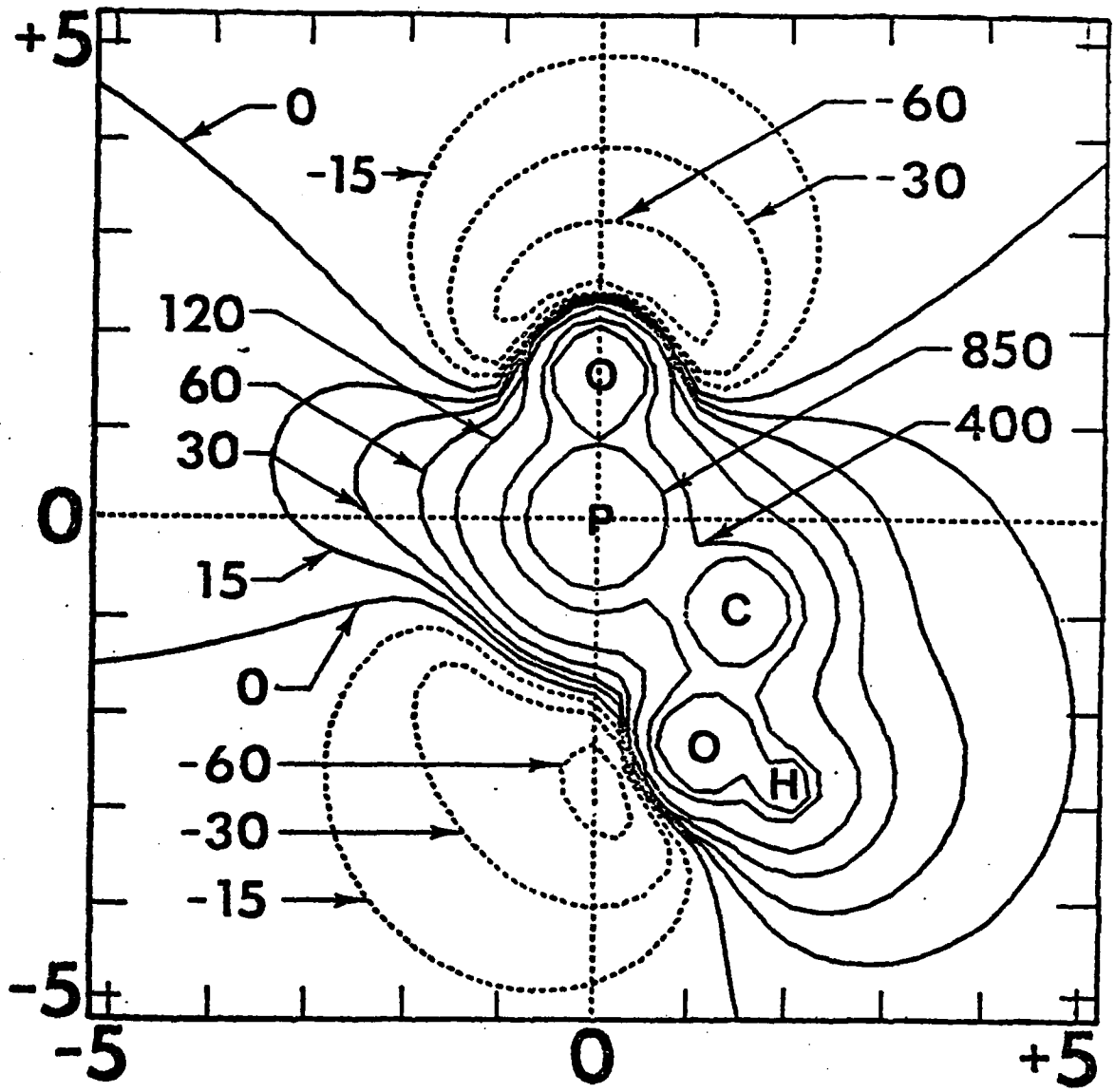

Fig. 10. Electrostatic potential contour plot for HMP in the plane of reflection symmetry using a 4-31G basis set. Potential values are in Kcal/mole and distances are in angstroms.

Table X(a). Calculated bond lengths and angles for PA.

Distance (Å)		Angles (degrees)	
P=O	1.50	O-P=O	116.53
P-O	1.55	P-O-H	110.32
O-H	1.00		

Table X(b). Calculated cartesian coordinates, in angstroms, for the atoms of PA.

Atom	x-coordinate	y-coordinate	z-coordinate
P	0.0	0.0	0.0
O	0.0	0.0	2.835
O	2.621	0.0	-1.309
H	3.999	0.0	-0.016
O	-1.309	-2.269	-1.312
O	-1.309	2.269	-1.312
H	-1.998	-3.464	-0.021
H	-1.998	3.464	-0.021

Table XI(a). Bond lengths and angles for MPA-E (eclipsed methyl group.)

Distance (Å)		Angles (degrees)	
P=O	1.50	C-P=O	122.21
P-O	1.55	C-P-O	100.88
O-H	1.00	O=P-O	113.30
C-P	1.78	P-O-H	110.38
C-H	1.10	O-P-O	103.98
		H-C-P	109.50
		H-C-H	109.43

Table XI(b). Calculated cartesian coordinates, in angstroms, for the atoms of MPA-E.

Atom	x-coordinate	y-coordinate	z-coordinate
P	0.0	0.0	0.0
O	0.0	0.0	2.835
O	2.690	0.0	-1.158
H	3.951	0.620	0.106
O	-1.269	2.373	-1.158
H	-1.316	3.776	0.106
C	-1.463	-2.441	-1.793
H	-2.302	-3.841	-0.505
H	-0.041	-3.369	-2.992
H	-2.952	-1.625	-2.992

Table XII(a). Calculated bond lengths and angles for MPA-S (staggered methyl group).

Distance (Å)		Angles (degrees)	
P=O	1.50	C-P=O	122.60
P-O	1.55	C-P-O	100.49
O-H	1.00	O=P-O	113.39
C-P	1.78	P-O-H	110.34
C-H	1.10	O-P-O	104.06
		H-C-P	109.50
		H-C-H	109.43

Table XII(b). Calculated cartesian coordinates, in angstroms, for the atoms of MPA-S.

Atom	x-coordinate	y-coordinate	z-coordinate
P	0.0	0.0	0.0
O	0.0	0.0	2.835
O	2.688	0.0	-1.163
H	3.957	0.573	0.115
O	-1.278	2.365	-1.163
H	-1.378	3.753	0.115
C	-1.451	-2.434	-1.812
H	-0.563	-4.259	-1.360
H	-1.210	-2.030	-3.836
H	-3.478	-2.521	-1.360

Table XIII(a). Calculated bond lengths and angles for HMP.

Distance (Å)		Angles (degrees)	
P=O	1.50	C-P=O	122.60
P-O	1.55	C-P-O	100.49
(P)-O-H	1.00	O=P-O	113.39
C-P	1.78	P-O-H	110.34
C-H	1.10	O-P-O	104.06
O-C	1.43	H-C-P	108.75
(C)-O-H	0.96	P-C-O	109.16
		C-O-H	104.34

Table XIII(b). Calculated cartesian coordinates, in angstroms, for the atoms of HMP.

Atom	x-coordinate	y-coordinate	z-coordinate
P	0.0	0.0	0.0
O	0.0	0.0	2.835
O	2.688	0.0	-1.163
H	3.957	0.573	0.115
O	-1.278	2.365	-1.163
H	-1.378	3.753	0.115
C	-1.451	-2.434	-1.812
H	-0.597	-4.256	-1.289
H	-3.460	-2.549	-1.289
O	-1.130	-1.895	-4.440
H	-1.952	-3.274	-5.285

AD-A135 304 ENVIRONMENTAL DURABILITY OF ALUMINUM ADHESIVE JOINTS PROTECTED WITH HYDRATION INHIBITORS(U) MARTIN MARIETTA LABS BALTIMORE MD G D DAVIS ET AL. NOV 83 2/2

UNCLASSIFIED MML-TR-83-34C N00014-80-C-0718 F/G 11/1 NL

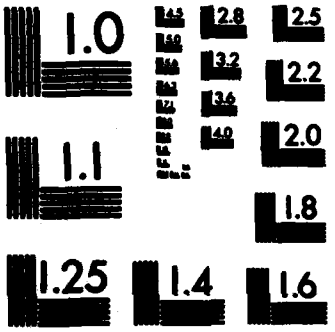

MICROCOPY RESOLUTION TEST CHART
NATIONAL BUREAU OF STANDARDS-1963-A

Table XIV. The atomic charges in PA, MPA, and HMP calculated by Mullikan population analysis and by the Potential Derived (PD) method using an STO-3G basis set. The bold face atoms in each entry in the left column are those of interest for that row. The other atoms in each entry indicate the neighbors.

Atom	Mullikan Population Charges				Potential Derived (PD) Charges			
	PA	MPA-E[a]	MPA-S[b]	HMP	PA	MPA-E[a]	MPA-S[b]	HMP
P	+1.47	+1.33	+1.34	+1.34	+1.86	+1.65	+1.69	+1.44
O-P	-0.62	-0.62	-0.62	-0.61	-0.79	-0.76	-0.77	-0.73
O-P	-0.48	-0.49	-0.49	-0.48	-0.64	-0.66	-0.66	-0.63
H-O	+0.20	+0.19	+0.19	+0.19	+0.29	+0.31	+0.31	+0.33
C-P		-0.37	-0.37	-0.19		-0.64	-0.77	-0.04
C **H**		+0.08	+0.08			+0.12	+0.21	
H H **C**		+0.09	+0.08			+0.16	+0.17	
H-**C**-**H**				+0.06				+0.03
C **O**				-0.29				-0.46
C-**O** **H**				+0.20				+0.33

a. Eclipsed methyl group
b. Staggered methyl group

Table XV. The atomic charges in PA, MPA, and HMP calculated by Mullikan population analysis and by the Potential Derived (PD) method using a 4-31G basis set. The bold face atoms in each entry in the left column are those of interest for that row. The other atoms in each entry indicate the neighbors.

Atom	Mullikan Population Charges				Potential Derived (PD) Charges			
	PA	MPA-E[a]	MPA-S[b]	HMP	PA	MPA-E[a]	MPA-S[b]	HMP
P	+2.29	+1.96	+1.94	+1.97	+2.17	+1.97	+2.03	+1.72
O=P	-0.97	-0.98	-0.98	-0.98	-0.98	-0.98	-0.99	-0.94
O-P	-0.92	-0.94	-0.93	-0.92	-0.88	-0.94	-0.96	-0.90
H-O	+0.48	+0.47	+0.47	+0.47	+0.48	+0.52	+0.52	+0.54
C-P		-0.79	-0.74	-0.29		-0.72	-0.87	+0.11
C **H**		+0.24	+0.25			+0.16	+0.27	
H H **C**		+0.25	0.23			+0.21	+0.21	
H-C-**H**				+0.22				+0.03
C **O**				-0.67				-0.72
C-**O** **H**				+0.41				+0.49

a. Eclipsed methyl group
b. Staggered methyl group

V. Conclusions

The initial results obtained by this project to use a combined experimental and theoretical approach in the application of IETS to the study of hydration inhibitors on aluminum oxide have clearly demonstrated the usefulness of the technique. The three main results from this work were as follows:

1. We developed a technique for consistently obtaining high quality IETS spectra for large phosphonate-based hydration inhibitors adsorbed in monolaywer coverages on aluminum oxide. We report spectra and analysis for three of these. These three revealed surface species which were strongly bonded to the oxide surface through the phosphonate group. The junction characteristics for a fourth indicated very weak bonding. It was determined independently to be a very poor inhibitor (MPA).

2. The "floating valence" tunneling model which we developed in order to analyze the IETS spectra of the inhibitor molecules is new. It represents a second generation model from our laboratory, and to our knowledge is the most accurate and tractable one in existance. The difficulty in applying it to the large inhibitor molecules is not an intrinsic shortcoming of the model itself, but is due instead to the fact that complete vibrational mode analyses have not been done—and perhaps never can be done adequately—on these molecules. Even the differences in the reported vibrational mode analyses for thiourea have caused us considerable problems.

3. The development and application of the floating valence model did produce an excellent spinoff. The sensitivity of this model to the partial atomic charge values in a molecule allowed us to evaluate several techniques for calculating these charges. The most accurate of these, the Potential Derived (PD) method, was used to calculate the atom charge distribution in three of the smaller phosphonate molecules.

4. By incorporating semi-empirical procedures the PD technique could be applied to molecules with 100 atoms. Such studies should be useful in evaluating the change in effectiveness of an inhibitor as different end groups are substituted onto the adsorbing group. It can be applied to a wide range of inhibitor types.

References

1. B.J. Van der Veken and M.A. Herman, J. Molecular Struct. 15, 225 (1973).

2. L.C. Thomas and Rosemary A. Chittenden, Spec. Acta 20, 489 (1964).

3. L.C. Thomas and Rosemary A. Chittenden, Spec. Acta. 20, 467, (1964).

4. John Kirtley, D.J. Scalapino, and P.K. Hausma, Phys. Rev B 14, 3177 (1976).

5. Frank A. Momany, J. Phys. Chem. 82, 592 (1978).

6. John Kirtley and James T. Hall, Phys. Rev. B 22, 848 (1980).

7. G.B. Aitken, J.L. Duncan, and G.P. McQuillan, J. Chem. Soc. (A), 2695 (1971).

8. J.E. Stewart, J. Chem. Phys. 26, 248 (1956).

9. D.F. McIntosh and M.R. Peterson, QCPE 11, 342 (1977).

10. P. Bleckmann, B. Schrader and W. Meier, Ber. Bunsenges. Phys. Chem. 75, 1279 (1971)

11. P.N. van Kampen, F.A.A.M. de Lacus, G.F. Smits and C. Altona, QCPE 13, 437 (1982)

END

FILMED

1-84

DTIC